BBA - Molecular Basis of Disease 1864 (2018) 1010–1023

Contents lists available at ScienceDirect

BBA - Molecular Basis of Disease

journal homepage: www.elsevier.com/locate/bbadis

# Dermal fibroblast-to-myofibroblast transition sustained by αvß3 integrin-ILK-Snail1/Slug signaling is a common feature for hypermobile Ehlers-Danlos syndrome and hypermobility spectrum disorders

Nicoletta Zoppi, Nicola Chiarelli, Silvia Binetti, Marco Ritelli, Marina Colombi*

*Division of Biology and Genetics, Department of Molecular and Translational Medicine, School of Medicine, University of Brescia, Brescia, Italy*

ARTICLE INFO

*Keywords:*
Hypermobile Ehlers-Danlos syndrome
Hypermobility Spectrum Disorders
Fibroblast-to-myofibroblast transition
αvβ3 integrin
Snail1/Slug
Chronic generalized inflammation

ABSTRACT

Hypermobile Ehlers-Danlos syndrome (hEDS) is a heritable connective tissue disorder with unknown molecular basis mainly characterized by generalized joint hypermobility, joint instability complications, and minor skin changes. The phenotypic spectrum is broad and includes multiple associated symptoms shared with chronic inflammatory systemic diseases. The stricter criteria defined in the 2017 EDS nosology leave without an identity many individuals with symptomatic joint hypermobility and/or features of hEDS; for these patients, the term Hypermobility Spectrum Disorders (HSD) was introduced. We previously reported that *in vitro* cultured hEDS and HSD patients' skin fibroblasts show a disarray of several extracellular matrix (ECM) components and dysregulated expression of genes involved in connective tissue homeostasis and inflammatory/pain/immune responses. Herein, we report that hEDS and HSD skin fibroblasts exhibit *in vitro* a similar myofibroblast-like phenotype characterized by the organization of α-smooth muscle actin cytoskeleton, expression of OB-cadherin/cadherin-11, enhanced migratory capability associated with augmented levels of the ECM-degrading metalloproteinase-9, and altered expression of the inflammation mediators CCN1/CYR61 and CCN2/CTGF. We demonstrate that in hEDS and HSD cells this fibroblast-to-myofibroblast transition is triggered by a signal transduction pathway that involves αvβ3 integrin-ILK complexes, organized in focal adhesions, and the Snail1/Slug transcription factor, thus providing insights into the molecular mechanisms related to the pathophysiology of these protean disorders. The indistinguishable phenotype identified in hEDS and HSD cells resembles an inflammatory-like condition, which correlates well with the systemic phenotype of patients, and suggests that these multisystemic disorders might be part of a phenotypic continuum rather than representing distinct clinical entities.

## 1. Introduction

Ehlers-Danlos syndromes (EDS) are a heterogeneous group of heritable connective tissue disorders (HCTDs) sharing a variable combination of skin hyperextensibility, generalized joint hypermobility (gJHM), internal organ and vessel fragility and dysfunctions. Thirteen EDS types are recognized by specific diagnostic criteria in the 2017 EDS nosology [1]. Classical EDS (cEDS), principally caused by mutations in *COL5A1* and *COL5A2* encoding type V collagen (COLLV), is characterized by cutaneous involvement and gJHM. Vascular EDS (vEDS), due to type III collagen (COLLIII) defects caused by *COL3A1* mutations, shows a marked fragility of blood vessels and internal organs. Hypermobile EDS (hEDS), a dominantly inherited trait without a defined molecular basis, is mainly defined by gJHM, joint dislocations/instability complications, *i.e.*, musculoskeletal chronic pain, and a combination of mucocutaneous features [1]. According to the 2017 EDS nosology, the following 3 criteria must be met for a hEDS diagnosis: gJHM, evaluated with an age-dependent Beighton score (criterion 1); two or more of the

*Abbreviations:* Ab, polyclonal antibody; α-SMA, α-smooth muscle actin; CE, cellular extract; cEDS, classical Ehlers-Danlos syndrome; CID, chronic inflammatory systemic diseases; CM, conditioned medium; COLLs, collagens; COLLIII, type III collagen; COLLV, type V collagen; DAMPs, danger/damage-associated molecular patterns; ECM, extracellular matrix; EDS, Ehlers-Danlos syndrome; EDS-HT, EDS hypermobility type; FN, fibronectin; gJHM, generalized joint hypermobility; HCTD, hereditary connective tissue disorder; hEDS, hypermobile Ehlers-Danlos syndrome; HRP, horseradish peroxidase; HSD, hypermobility spectrum disorders; IF, immunofluorescence microscopy; ILK, integrin linked kinase; JHS, joint hypermobility syndrome; mAb, monoclonal antibody; MEM, Earle's Modified Eagle Medium; MMP, matrix metalloproteinase; O.N., over night; PFA, paraformaldehyde; qPCR, quantitative real-time polymerase chain reaction; SEM, standard error of mean; R.T., room temperature; UM, unconditioned medium; vEDS, vascular Ehlers-Danlos syndrome; WB, Western blotting

* Corresponding author at: Division of Biology and Genetics, Department of Molecular and Translational Medicine, School of Medicine, University of Brescia, Viale Europa 11, 25123 Brescia, Italy.

*E-mail address:* marina.colombi@unibs.it (M. Colombi).

https://doi.org/10.1016/j.bbadis.2018.01.005
Received 28 July 2017; Received in revised form 5 December 2017; Accepted 2 January 2018
Available online 05 January 2018
0925-4439/ 

following features: systemic manifestation of a more generalized soft HCTD, family history, complications of gJHM (criterion 2); and absence of unusual skin fragility, exclusion of other heritable and acquired CTDs, such as autoimmune rheumatologic conditions, and other alternative diagnoses (criterion 3) [1]. This new set of clinical criteria is stricter than the previous Villefranche criteria, used for the diagnosis of EDS hypermobility type (EDS-HT) [2], and the Brighton criteria for joint hypermobility syndrome (JHS) [3]. For all those phenotypes presenting symptomatic JHM plus one or more of its secondary manifestations, but that do not fulfill the new hEDS criteria, the term hypermobility spectrum disorder(s) (HSD) was introduced to not leave patients with an incomplete clinical presentation without a defined diagnosis [4]. In the recent years, the hEDS-associated phenotypic spectrum was complicated by the description of multiple associated manifestations not comprised in the new diagnostic criteria for hEDS that include gastrointestinal dysfunction, increased susceptibility to osteoarthritis, chronic generalized musculoskeletal pain, inflammatory soft-tissue lesions, and a range of neurological features, *i.e.*, myalgia, cramps, sickness behavior/fatigue/depressive symptoms, and sleep disturbance [1,4–6]. Many of these features are typical symptoms of chronic inflammatory systemic diseases (CID), such as rheumatoid arthritis, systemic lupus erythematosus, multiple sclerosis, and ankylosing spondylitis [7], which must be excluded during the diagnostic process of a hEDS patient according to the criterion 3 of the new nosology [1].

In hEDS and HSD patients' skin fibroblasts, we previously reported a widespread disarray of several extracellular matrix (ECM) structural components, such as type I collagen, COLLIII, and COLLV, fibronectin (FN), fibrillins, tenascins, and elastin, together with a dysregulated expression of many genes related to ECM organization, cell adhesion, immune and inflammatory responses [8]. hEDS and HSD fibroblasts also do not organize the COLL- and FN-specific α2β1 and α5β1 integrin receptors [8], but express the αvβ3 integrin that is a common trait of all types of EDS fibroblasts [8–12].

Fibroblasts are primarily responsible for synthesis, remodeling, and reabsorption of ECM in tissues, and through synthesis of cytokines and chemokines modify the quality and duration of the inflammatory responses [13]. At the end of these responses, they contribute to the resolution of inflammation, mostly normalizing the chemokine gradients and allowing infiltrating leukocytes to undergo apoptosis [14]. Fibroblasts can be activated by a variety of autocrine and paracrine signals for their transition to myofibroblasts [15]. These specialized cells show fibroblast and smooth muscle cell-like characteristics and are involved in the contraction of ECM during wound healing [16], in pathological conditions such as fibrosis [17], and contribute to chronic inflammation [18]. In response to injury, myofibroblasts are activated by inflammatory cytokines and mediators produced by local cells. Phenotypic changes occurring in fibroblast-to-myofibroblast transition include the expression of the α-smooth muscle actin (α-SMA) and its incorporation into stress fibres that allows cell's migration and contraction [19,20]. These structures are directly connected at sites of cadherin-cell adherens junctions; indeed, during the fibroblast-to-myofibroblast transition a decrease of N-cadherin expression and an increase of OB-cadherin/cadherin-11 have been described [21]. Myofibroblasts also synthesize and secrete cytokines, ECM molecules, such as COLLs and FN, and matrix metalloproteinases (MMPs) that control the ECM turnover and remodeling [22,23]. Furthermore, during tissue repair, growth factors are induced by tissue injury and inflammation including CCN2/CTGF and CCN1/CYR61 that have respectively a stimulatory and antagonist effect on myofibroblasts proliferation and differentiation and on the resolution phase of the inflammatory state [24,25]. When the myofibroblasts' activity persists, unsuccessful repair occurs and chronic contractures and/or fibrosis develop [26]. Presence of myofibroblasts, or myofibroblast-like contractile cells, has been demonstrated in several tissues during inflammation including synovia of ligaments, menisci, and tendons [27].

In this work, we report that cultured skin fibroblasts derived from hEDS and HSD patients show a myofibroblast-like phenotype in the presence of α-SMA and OB-cadherin/cadherin-11 organization, enhanced active MMP-9 levels, and increased expression of CCN2/CTGF and demonstrate an ILK-mediated αvβ3 integrin pathway that signals to Snail1/Slug to regulate this fibroblast-to-myofibroblast transition.

## 2. Materials and methods

### 2.1. Patients, skin biopsies, and ethical statement

Skin biopsies from 4 hEDS, 3 HSD, 4 cEDS, 4 vEDS patients, and 2 unrelated age-matched healthy donors, were established in our lab by standard protocols, following approval by the local Ethical Committee "Comitato Etico di Brescia, ASST Spedali Civili, Brescia, Italia" (registration numbers NP2378, and NP2658). All patients were diagnosed at the Centre of Heritable Connective tissue disorders and EDS of the University Hospital Spedali Civili of Brescia.

Among the hEDS (hEDS P1, P2, P3, P4) and HSD (HSD P5, P6, P7) patients, 5 were previously reported in Chiarelli et al. [8], which were re-classified following the 2017 EDS nosology [1], and 2 were novel patients. Six were females with an age range on examination of 34 to 53 years, and a 36-year-old male. The corresponding patients' identifier, their classification according to the revised and the Villefranche nosology, and the Brighton criteria, and the detailed description of mucocutaneous, osteoarticular, orthopedic, muscular, gastrointestinal, cardiovascular, neuropsychiatric, uro-gynecological, immunological, and ocular signs are summarized in Supplementary Table 1.

The 4 cEDS fibroblasts analyzed here (cEDS P1, P2, P3, P4) derived from patients previously described in Ritelli et al. [28] as AN_002514, AN_002503, and AN_002526, harboring the c.2988del (p.Gly997Alafs*77), c.1165-2A > G (p.Pro389Leufs*168), c.4178G > A (p.Gly1393Asp) *COL5A1* mutations, respectively, and as AN_002534 carrying the c.2499 + 2T > C (p.Gly816_Pro833del) *COL5A2* mutation. Similarly, the 4 vEDS patients for whom skin fibroblasts were obtained (vEDS P1, P2, P3, and P4 this study) were previously reported in Drera et al. [29] as P.1, P.2, P.4, and P.10, respectively. All these patients carried a structural *COL3A1* mutation, *i.e.*, c.764G > A (p.Gly225Asp), c.709G > A (p.Gly237Arg), c.951 + 6T > C (p.Gly301_Ala318del), and c.1835G > A (p.Gly612Asp), respectively.

### 2.2. Cell cultures, antibodies, and inhibitors

Skin fibroblasts from healthy donors, hEDS, HSD, cEDS and vEDS patients were grown *in vitro* at 37 °C in a 5% $CO_2$ atmosphere in Earle's Modified Eagle Medium (MEM) supplemented with 2 mM L-glutamine, 10% FBS (Corning Life Sciences, B.V., Amsterdam, The Netherlands), and 100 μg/ml penicillin and streptomycin (Life Technologies, Carlsbad, CA, USA). Cells were expanded until full confluency and then harvested by 0.25% trypsin/0.02% EDTA treatment at the same passage number (from 1st to 10th). In addition, control fibroblasts were grown for 10 days in the presence of conditioned media (CM) recovered from 72 h-grown control, hEDS, HSD, and cEDS fibroblasts' cultures and replenished every 48 h. Protein concentration of CM was evaluated using detergent compatible Bio-Rad $D_c$ Protein Assay (Bio-Rad Laboratories, Hercules, CA, USA) and a concentration of 2.5 mg/ml was used in the experiments.

ILK inhibition was performed growing for 18 h control, hEDS, and HSD cells in MEM supplemented with 5% FBS in the absence and in the presence of increasing concentrations, from 0.5 to 4.0 μM, of Cpd22 inhibitor.

The mouse anti-αvβ3 (clone LM609) integrin monoclonal antibody (mAb) recognizing integrin ligand-binding sites, the mouse anti-β3 integrin subunit (clone B3A), the affinity purified rabbit polyclonal antibody (Ab) against the β3 integrin subunit, and the inhibitory compound Cpd22 were from Millipore-Chemicon Int. (Billerica, MA, USA).

The rabbit Ab against all human isoforms of FN, the anti-α-SMA mAb (clone 1A4), the mAb against β-actin (clone AC-74), the horseradish peroxidase (HRP)-conjugated anti-rabbit, and anti-mouse secondary Abs were from Sigma Chemicals (St. Louis, MO, USA). The anti-human ILK mAb (clone 65.1.9) was from Upstate (Lake Placid, NY). The anti-human paxillin mAb (clone 165) was from BD Biosciences (Milan, Italy). Rabbit Abs against the human Snail1/Slug, the MMP-9, the anti-β1 integrin subunit (clone BV7) mAb, and the RabMab rabbit anti-ILK mAb (clone EP1593Y) were from Abcam Ltd. (Cambridge, UK). The mouse anti-lamin A/C mAb (clone mab636) was from Thermo Fisher Scientific (Waltham, MA USA). The rabbit anti-CCN1/CYR61 Ab was from LSBio LifeSpan BioSciences, Inc. (Seattle, WA, USA). The Alexa Fluor® 488 anti-rabbit and the Alexa Fluor® 594 anti-mouse Abs, the rabbit anti-CDH11/Cadherin OB, and anti-CCN2/CTGF Abs were from Life Technologies. The rabbit anti-integrin β3 $pY^{773}$ phosphospecific Ab was from Biosource Int. Inc. (Camarillo, CA, USA). The mouse anti-GAPDH (clone 0411) mAb was from Santa Cruz Biotechnology, INC. (Heidelberg, Germany).

### 2.3. Quantitative real-time PCR

Relative expression levels of *MMP9* and *SNAIL1* were evaluated by quantitative real-time PCR (qPCR). 3 μg of total RNA from 4 hEDS, 2 HSD, 4 cEDS skin fibroblasts and 2 unrelated healthy controls were reverse-transcribed with random primers by standard procedure. qPCR reactions were performed with the ABI PRISM 7500 Real-Time PCR System by standard thermal cycling conditions and by using SYBR Green qPCR Master Mix (Life Technologies), 10 ng of cDNA, and with 10 μM of each primers set. *GAPDH* and *YWHAZ* reference genes were amplified for normalization of cDNA loading. All qPCR reactions were run in triplicate. Relative mRNA expression levels were normalized to the geometric mean of the reference genes and analyzed using the $2^{-(\Delta\Delta Ct)}$ method. Results were expressed as the mean value of relative quantification ± standard error of mean (SEM). Statistical significance between EDS compared to control cells was determined using an unpaired Student's *t*-test with the GraphPad Prism software (GraphPad Software, Inc., La Jolla, CA, USA).

### 2.4. Cell migration assay

The migratory potential of control, cEDS, vEDS, hEDS and HSD cells under basal conditions, and of control fibroblasts plated either in the presence of their own CM, or of CM recovered from cEDS, hEDS and HSD cells was analyzed using the Transwell 8-μm filter (Corning Costar, Cambridge, MA) migration assay. $5 \times 10^4$ control and EDS skin fibroblasts, resuspended in serum-free MEM, were plated into the upper chamber, and allowed to migrate for 6 h through the polycarbonate filter into the bottom well. The bottom wells were filled with unconditioned complete MEM (UM) or with control, cEDS, hEDS and HSD cells' CM. Non-migrated cells were removed from the upper surface using a cotton swab. Migrated cells collected in the bottom chamber were methanol-fixed and stained with Diff-Quick staining kit (Medion Diagnostic GmbH, Switzerland), following manufacturer's instructions. Migration was quantified by counting the cells in ten 1 $mm^2$ non-overlapping fields using a light microscope. Statistical significance was determined using one-way ANOVA followed by Dunnett's multiple comparisons *post hoc* test. Data are expressed as means ± SEM from 3 independent experiments performed in triplicate. Analyses were performed with GraphPad Prism software.

### 2.5. Immunofluorescence microscopy (IF)

To analyze αvβ3 integrin, β1 integrin subunit, and ILK distribution, control, cEDS, vEDS, hEDS, and HSD cells, grown for 72 h on glass coverslides were fixed in 3% paraformaldehyde (PFA)/60 mM sucrose and permeabilized in 0.5% (v/v) Triton X-100 as previously reported [9]. In particular, fibroblasts were reacted for 1 h at room temperature (R.T.) with 4 μg/ml anti-αvβ3 integrin, anti-β1 subunit, and anti-ILK mAbs diluted in 1% BSA. The co-distribution of the αvβ3 integrin with ILK protein was evaluated performing a double staining of the cells, in the same conditions and immunoreacting with 1:50 anti-β3 $pY^{773}$ integrin subunit Ab and anti-ILK mAb as reported above. Alternatively, control fibroblasts were grown for 10 days in the absence or in the presence of CM recovered from 72 h-grown control, cEDS, hEDS, and HSD fibroblasts' cultures, replenished every 48 h, and immunoreacted as mentioned above with anti-αvβ3 mAb, and with 2 μg/ml anti-paxillin mAb. Cells grown in the same conditions and fixed in cold methanol were immunoreacted for 1 h with 1:50 anti-α-SMA mAb diluted in 1% BSA or with 1:100 anti-FN Ab diluted in 0.3% BSA. To analyze Snail1/Slug distribution, 72 h-grown control, cEDS, hEDS, HSD cells, and control fibroblasts, grown for 10 days in the presence of CM recovered from 72 h-grown control, cEDS, hEDS, and HSD fibroblasts' cultures, were fixed for 15 min in 3.7% PFA/60 mM sucrose, blocked 30 min with 0.1% non-fat milk/0.1% Tween 20/PBS 1x, and immunoreacted with 1:500 anti-Snail1/Slug Ab diluted in 0.1% Tween 20/PBS 1 × O.N. at + 4 °C.

To investigate the expression of CCN1/CYR61, 72 h-grown control, cEDS, hEDS, and HSD cells were fixed with 4% PFA for 20 min, permeabilized with 0.3% Triton X-100 for 5 min, blocked with 50% FBS/1% BSA/0.025% Tween 20/PBS 1x for 30 min at 37 °C, and immunoreacted O.N. at + 4 °C with the specific rabbit anti-CCN1/CYR61 Ab diluted 1:100 in 1% BSA. The expression of OB-cadherin/cadherin-11 was investigated fixing control and EDS cells in 4% PFA/10 mM sucrose for 10 min, permeabilizing with 0.1% Triton X-100 for 10 min and blocking in 2% BSA/PBS 1x for 1 h at R.T.; cells were then immunoreacted for 3 h at R.T. with 2 μg/ml rabbit anti-CDH11/Cadherin OB Ab diluted in 0.1% BSA. The analysis of the effects of ILK inhibition on ILK, αvβ3 integrin, α-SMA and Snail1/Slug distribution was performed on control, hEDS, and HSD cells grown for 18 h in the absence and in the presence of increasing concentrations (0.5, 1.0, 2.0, 3.0, 4.0 μM) of Cpd22 compound; the cells were fixed and immunoreacted with anti-ILK, anti-αvβ3 integrin, and anti-α-SMA mAbs and with anti-Snail1/Slug Ab, as reported above. Cells were incubated for 1 h with anti-mouse or anti-rabbit secondary Abs conjugated to Alexa Fluor® 594 and 488, respectively. IF signals were acquired by a CCD black-and-white TV camera (SensiCam-PCO Computer Optics GmbH, Germany) mounted on a Zeiss fluorescence Axiovert microscope and digitalized by Image Pro Plus software (Media Cybernetics, Silver Spring, MD, USA). All experiments were repeated three times.

### 2.6. Cell extracts, immunoprecipitation, and Western blotting (WB)

To analyze FN, MMP-9, CCN1/CYR61, and CCN2/CTGF secreted in the cell medium, control, cEDS, hEDS, and HSD cells were cultured in complete medium for 72 h and CM were collected in the absence and in the presence, respectively, of proteases inhibitors, 1 mM PMSF, 1 mM aminobenzamidine and 50 mM EDTA after centrifugation. CCN1/CYR61 and CCN2/CTGF were analyzed in the cell extract (CE) obtained by cell lysis at + 4 °C with RIPA buffer treatment (20 mM Tris-HCl pH 7.2, 150 mM NaCl, 2% NP-40, 0.1% SDS, 0.5% DOC, 1 mM PMSF, 1 mM aminobenzamidine, 25 mM EDTA, 10 μg/ml leupeptin, 4 μg/ml pepstatin, 0.1 UI/ml aprotinin) and centrifuged at 13,000 rpm at + 4 °C for 10 min. The protein concentration was evaluated using detergent compatible Bio-Rad $D_c$ Protein Assay and 25 μg of total proteins were separated in reducing conditions by electrophoresis using 8% SDS-PAGE. After nitrocellulose sheet transfer, the membranes were blocked O.N. at 37 °C with 3% and 5% non-fat dry milk in PBS 1x, respectively, and immunoreacted with 1:1000 anti-FN Ab diluted in 0.3% BSA or with 1:1000 anti-CCN1/CYR61 and anti-CCN2/CTGF Abs diluted in 2.5% milk/TBS-0.1% Tween 20 (TBS-T) for 3 h at R.T. After stripping, the CE filter was reprobed with 2 μg/ml anti-β actin mAb, as loading control. To analyze the secretion of MMP-9, 150 μg of proteins were

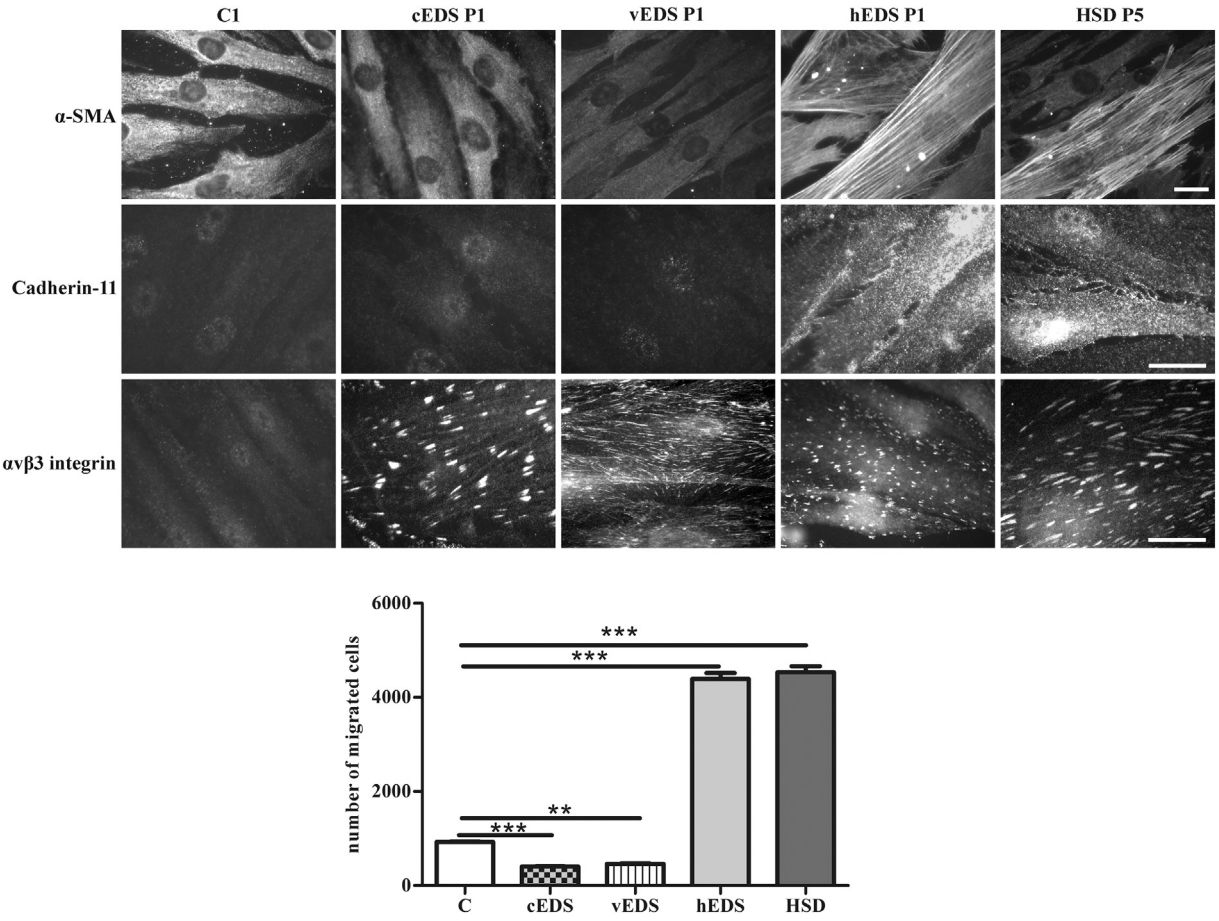


**Fig. 1. The organization of α-SMA, OB cadherin/cadherin-11, αvβ3 integrin, and the increased migratory activity in hEDS and HSD cells are consistent with a fibroblast-to-myofibroblast transition**. IF of α-SMA cytoskeleton, OB cadherin/cadherin-11, and αvβ3 integrin in 72 h-grown control C1, cEDS P1, vEDS P1, hEDS P1, and HSD P5 dermal fibroblasts. The cells were analyzed at different *in vitro* cell growth passages ($1^{st}$–$10^{th}$) with similar results (not shown).

The images represent cell strains analyzed at $5^{th}$ *in vitro* passage and are representative of 2 controls, 4 cEDS, 4 vEDS, 4 hEDS, and 3 HSD cell strains (see Supplementary Fig. 1). Scale bars: 10 μm. The number of migrated cells in 10 1 $mm^2$ non-overlapping microscopic fields were counted for each cell strain. Data shown represent the means ± SEM from 3 independent experiments performed in triplicate for 2 controls, 4 cEDS, 4 vEDS, 4 hEDS, and 3 HSD cell strains (**P < 0.01; **P < 0.001 compared with control cells).

separated in not-reducing conditions by 8–10% SDS-PAGE; immunoblotting was performed by saturating the nitrocellulose membrane O.N. at 37 °C in PBS/5% non-fat milk and incubating for 4 h at R.T. with the rabbit anti-MMP-9 Ab recognizing both the pro-form (95 kD) and the active form (82 kD) of the human enzyme (dilution 1:1000 in PBS/3% non-fat milk). After washing in TBS-T, membranes were incubated for 2 h at R.T. with HRP-conjugated anti-rabbit IgGs, diluted in 0.3% BSA and 2.5% milk/TBS-T, respectively, and developed using the ECL method (Pierce).

The membrane-bound αvβ3 integrins were extracted by lysing cells with 0.5% Triton X-100, 150 mM NaCl, 1 mM $CaCl_2$, 1 mM $MgCl_2$, 20 mM Tris-HCl pH 7.4, 1 mM $Na_3VO_4$, 10 mM NaF, 10 mM $Na_4P_2O_7$, 1 μg/ml leupeptin, 4 μg/ml pepstatin, 0.1 UI/ml aprotinin. To analyze αvβ3 integrin co-precipitation with ILK and Snail1/Slug, 1 mg of proteins from control, hEDS, and HSD cells was immunoprecipitated with 10 μg of anti-αvβ3 mAb in accordance with the immunoprecipitation dynabeads protein G kit instructions (Novex by Life Technologies). Immunocomplexes were tested by WB in a 4–8% non-reducing gel, immunoreacting the 5% non-fat dry milk-blocked filter with 1 μg/ml anti-β3 integrin subunit Ab. The filter was stripped, tested for the absence of a residual signal and reprobed with 1 μg/ml anti-ILK mAb and then with 1:1000 anti-Snail1/Slug Ab. Primary Abs were diluted in 5% non-fat milk/TBS-T and incubated 3 h at R.T. After washing in TBS-T, the membrane was incubated for 2 h at R.T. with 1:500 HRP-conjugated anti-rabbit or anti-mouse IgGs, diluted in TBS-T and developed using the ECL method. Alternatively, total β3 integrin subunit, ILK, and Snail1/Slug recovered from control, hEDS, and HSD cells' extracts were analyzed as reported above. The two stripped filters were reprobed with 1 μg/ml anti-GAPDH mAb, as negative control of immunoprecipitation and as loading control, respectively. To analyze the ILK-mediated interaction of Snail1/Slug with αvβ3 integrin, ILK was extracted from control, hEDS, and HSD cells with 10 mM Tris-HCl pH 7.4, 1% Triton X-100, 150 mM NaCl, 1 mM EDTA, 1 mM $Na_3VO_4$, 10 mM NaF, 10 mM $Na_4P_2O_7$, 10 μg/ml leupeptin, 4 μg/ml pepstatin, 0.1 UI/ml aprotinin. One mg of each cell extract was immunoprecipitated for 1 h with 4 μg anti-ILK RabMab and the immunocomplexes were tested in a 4–8% gel and immunoreacting the 5% non-fat dry milk-blocked filter with 1 μg/ml anti-ILK mAb and 1:1000 diluted anti-Snail1/Slug Ab. The extraction of total Snail1/Slug was performed by scraping untreated and Cpd22-treated control, cEDS, hEDS, and HSD cells in the extraction buffer containing 20 mM Tris-HCl pH 8.0, 250 mM NaCl, 2 mM EDTA, 0.1% Triton X-100, 4 mM $Na_3VO_4$, 5 mM NaF and 5 mM $Na_4P_2O_7$, 5 μg/ml leupeptin, 10 μg/ml aprotinin, and 0.4 mM PMSF. The nuclear fraction of Snail1/Slug was obtained by REAP method, as previously described [30]. In particular, untreated and Cpd22-treated cells grown as monolayers in 10 cm diameter dishes were washed in ice-cold PBS pH 7.4, scraped from culture dishes on ice and collected in 1 ml of ice-cold PBS. After centrifugation, supernatants were removed and cell pellets were resuspended in 900 μl of ice-cold 0.1% NP40 (Calbiochem, CA, USA) in PBS, triturated 5 times using a micropipette, and centrifuged; the supernatant was removed as the cytosolic fraction. The pellet was resuspended in 1 ml of ice-cold 0.1% NP40 in PBS and

centrifuged, and the supernatant was discarded. The pellet of the nuclear fraction (about 20 μl) was resuspended in 180 μl of 1 × Laemmli sample buffer and sonicated twice for 5 s, followed by boiling for 1 min. 25 μg of total and nuclear proteins were separated by electrophoresis using 8–12% SDS-PAGE and filters were immunoreacted with the anti-Snail1/Slug Ab. Filters of total and nuclear cell extracts were stripped, tested for the absence of a residual signal and reprobed with 2 μg/ml anti-β-actin and anti-lamin A/C mAbs, respectively, as loading controls. To ensure the specificity of the nuclear extract, the filter was reacted with anti-β-actin mAb. Each experiment was performed two times.

## 3. Results

### 3.1. hEDS and HSD dermal fibroblasts exhibit a myofibroblast-like phenotype

Control, cEDS, vEDS, hEDS, and HSD dermal fibroblasts were analyzed by IF for the expression and organization of α-SMA, OB-cadherin/cadherin-11, and αvβ3 integrin. As shown in Fig. 1 and **Supplementary Fig. 1**, hEDS and HSD cells organized α-SMA in cytoskeletal stress fibres, whereas control, cEDS and vEDS cells showed, at different levels, disorganized α-SMA in the cytoplasm and perinuclear region. The α-SMA cytoskeleton was detectable at each *in vitro* passage, starting from the 1$^{st}$ to the 10$^{th}$. The percentage of cells organizing the α-SMA cytoskeleton ranged from about 60% to 90% in the different hEDS and HSD cell strains, without any difference between the two cell types and *in vitro* passage (not shown). Similarly, OB-Cadherin/Cadherin-11 was highly expressed and organized in cytoplasmic bridges only by hEDS and HSD cells (Fig. 1, **Supplementary Fig. 1**). The αvβ3 integrin was organized on the whole surface of all EDS cells, both in fibrillar and focal adhesions in different shaped-patches, whereas it was almost absent in control fibroblasts (Fig. 1, **Supplementary Fig. 1**). The expression in both hEDS and HSD cells of α-SMA and OB-cadherin/cadherin-11, which are myofibroblasts' markers, prompted us to evaluate the migratory potential of these cells by Transwell assay. Indeed, the number of migrated hEDS and HSD cells was about 5-fold higher than that of control fibroblasts. On the contrary, cEDS and vEDS cells showed a diminished migration of about 2-fold (Fig. 1). Overall, these data demonstrate that both hEDS and HSD fibroblasts exhibit *in vitro* a myofibroblast-like phenotype with an enhanced migratory capability, which distinguishes them from cEDS and vEDS cells. Given the comparable cellular phenotype of hEDS and HSD cells, the subsequent experiments were performed only on 2 hEDS (P1, P2) and 2 HSD (P5, P6) cell strains at the 5$^{th}$ *in vitro* growth passage. In addition, since also cEDS and vEDS exhibit a similar cellular behavior, only cEDS skin fibroblasts were further included in the study.

### 3.2. hEDS and HSD cells secrete factors promoting fibroblast-to-myofibroblast transition

To verify whether *in vitro* grown hEDS and HSD cells release factors promoting the fibroblast-to-myofibroblast transition, control fibroblasts were grown in the presence of CM recovered from control, cEDS, hEDS, and HSD cells grown for 72 h, and the α-SMA cytoskeleton assembly was analyzed. In the presence of control and cEDS fibroblasts' CM, the cells showed a reduction of the α-SMA protein (Fig. 2A), whereas in the presence of CM recovered from hEDS and HSD cell strains from 40% to 85% of cells organized α-SMA stress fibres (Fig. 2A). Subsequently, the control fibroblasts' migration towards different CM was measured by Transwell assay. As shown in Fig. 2B, control fibroblasts exhibited an increased migratory activity (about 4-fold higher compared with UM) only in the presence of hEDS and HSD cells' CM. Together, these findings show that only hEDS and HSD cells secrete molecules able to promote the migratory myofibroblast-like phenotype.

To verify whether hEDS and HSD cells specifically express factors promoting inflammation that might be involved in the fibroblast-to-myofibroblast transition, the inflammatory proteins CCN1/CYR61 and CCN2/CTGF were analyzed by IF and/or WB. Control and cEDS cells abundantly expressed and organized on the plasma membrane CCN1/CYR61, which was also secreted in the media (Fig. 2C). Conversely, in hEDS and HSD cells CCN1/CYR61 was undetectable in CE and present at low levels in their media (Fig. 2C). CCN2/CTGF was present in the culture media of hEDS and HSD cells at levels comparable to those observed in control and cEDS cells, whereas in the CE it was found at higher amounts (Fig. 2C).

Since ECM molecules or their fragments released by MMPs activated in response to injury are known to be pro-inflammatory signals *in vivo*, the ECM organization of FN and the possible presence of its proteolytic fragments were investigated in cEDS, hEDS, and HSD cells by IF and WB. In line with our previous studies [8,9], IF analysis showed that all EDS cell types did not organize a fibrillar FN-ECM (Fig. 2D). WB demonstrated that degraded FN proteolytic fragments are present only in hEDS and HSD cells' media (Fig. 2D), suggesting the occurrence of a proteolytic activity. This hypothesis was corroborated by the treatment of control fibroblasts with CM from all cell types, which induced the disorganization of the FN-ECM only in the presence of hEDS and HSD cells' CM (Fig. 2D). Consequently, the expression of the ECM-degrading MMP-9 was investigated by qPCR and WB that showed an increase of both mRNA and protein levels in hEDS and HSD compared to control and cEDS fibroblasts (Fig. 2D). In hEDS and HSD cells media the MMP-9 82 kDa active form was present at high levels, whereas only the inactive 95 kDa proenzyme was secreted by control fibroblasts, suggesting an increased proteolytic activity of this protease in hEDS and HSD media. In cEDS cells, the MMP-9 protein was almost undetectable, consistent with the 3-fold lower mRNA levels detected by qPCR compared to control cells (Fig. 2D). Overall, these data highlight that hEDS and HSD cells display a range of phenotypic features that are typical of myofibroblasts.

### 3.3. The αvβ3 integrin transduces through ILK in the focal adhesions for the organization of the α-SMA cytoskeleton

To investigate the possible involvement of the αvβ3 integrin organized in hEDS and HSD cells in the establishment of their α-SMA cytoskeleton, first, a 10-days treatment of control fibroblasts with hEDS and HSD cells' CM was performed. Control fibroblasts, grown in the presence of their own CM and of that recovered from cEDS cells, did not recruit the αvβ3 integrin as well as under basal conditions. In contrast, the treatment with both hEDS and HSD cells' CM, promoting the α-SMA assembly (Fig. 2A), induced the organization of abundant αvβ3 integrin patches, preferentially localized in focal adhesions (Fig. 3A).

To better define the possible involvement of an αvβ3 integrin-mediated signal transduction pathway in hEDS and HSD cells, the expression of ILK, which in skin fibroblasts can interact with the cytoplasmic domain of the β1 and β3 integrin subunits and is known to be involved in migration and transdifferentiation mechanisms [31], was investigated. In control, cEDS, hEDS and HSD cells ILK was detected by IF with a different localization, *i.e.*, in focal and fibrillar adhesions in control and cEDS fibroblasts and mainly in focal adhesions in hEDS and HSD cells (Fig. 3B). Subsequently, the co-immunoprecipitation of αvβ3 integrin with ILK and the total levels of αvβ3 and ILK were analyzed in CE of control, hEDS and HSD cells (Fig. 3B, **Supplementary Fig. 2**). cEDS fibroblasts were not included, since in these cells we previously demonstrated an ILK-independent αvβ3 transduction pathway involving paxillin- and p60Src [10]. As shown in Fig. 3B, hEDS and HSD cells immunoprecipitated higher amounts of β3 integrin subunit and ILK than control fibroblasts, suggesting that this kinase co-localizes with the αvβ3 integrin. We next investigated the αvβ3 integrin activation through IF by analyzing the phosphorylation of Tyr 773 (pY$^{773}$) in the β3 integrin subunit. Indeed, only in hEDS and HSD cells the β3 integrin subunit in focal adhesions was activated and co-localized with ILK (Fig. 3C). In control cells, ILK in fibrillar and focal adhesions should co-

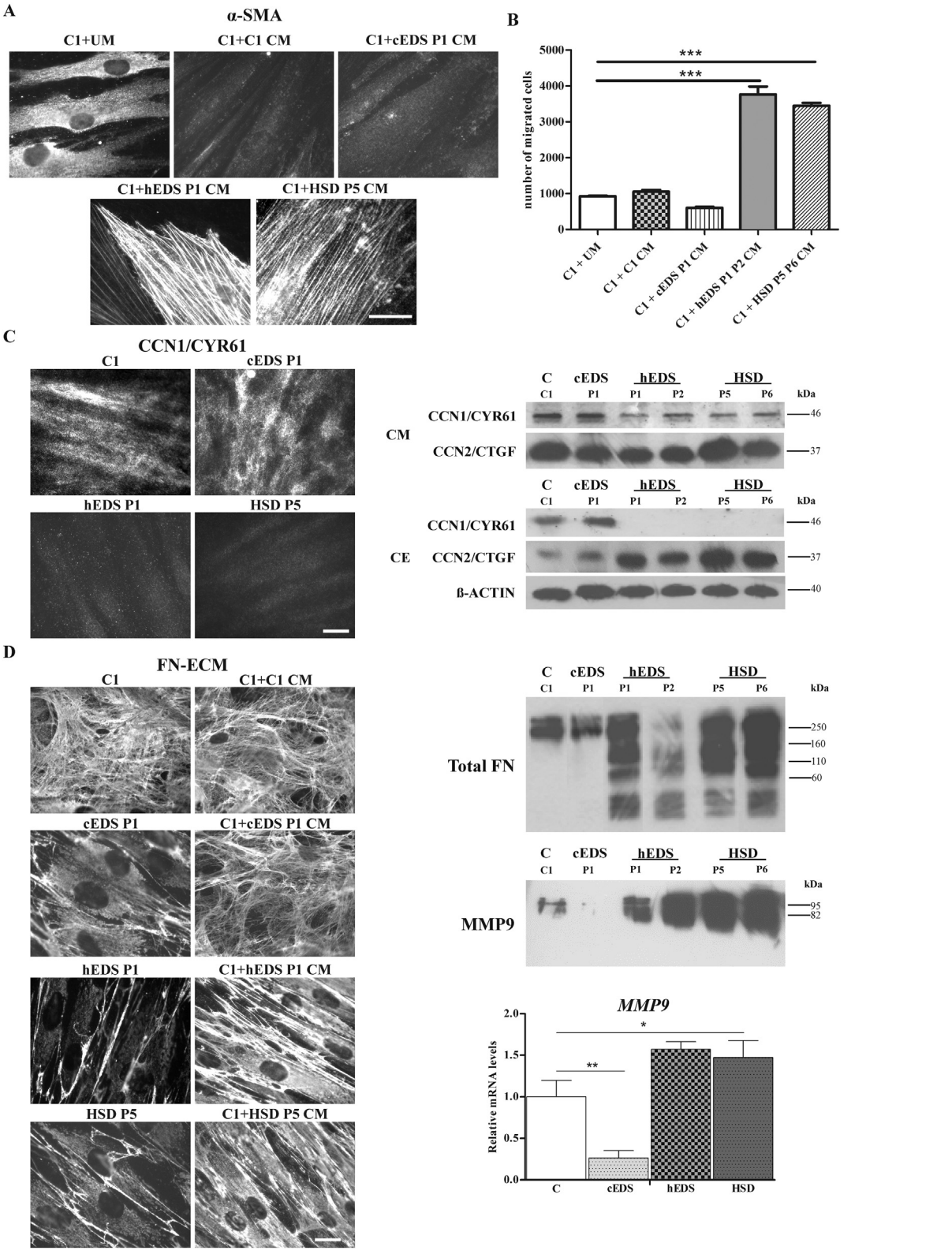


*(caption on next page)*

localize with the β1 integrin subunit, for instance with the canonical FN- and COLLs- receptors α5β1 and α2β1 respectively, which are abundantly expressed in these cells [10]. In hEDS and HSD cells, we previously demonstrated that they did not organize the α5β1 and α2β1 dimers [8]. To exclude the expression of other β1-containing integrins that are expressed in skin fibroblasts, *i.e.*, dimers containing αv or different α integrin partners including α1, α4, α7, and α9, the organization of β1 integrin subunit was analyzed by IF that demonstrated the lack of expression of this integrin subunit both in hEDS and HSD cells (**Supplementary Fig. 3**).

ILK localization was also investigated in control fibroblasts treated with different CM. As shown in Fig. 3D, control cells, treated with their

**Fig. 2. hEDS and HSD cells secrete factors promoting fibroblast-to-myofibroblast transition.**
(**A**) IF of the α-SMA cytoskeleton assembly in control fibroblast (C1) grown for 10 days in the presence of UM (C1 + UM), its own CM (C1 + C1 CM), and CM obtained from cEDS P1 (C1 + cEDS P1 CM), hEDS P1 (C1 + hEDS P1 CM), and HSD P5 (C1 + HSD P5 CM) cells. Comparable results were obtained by using CM of hEDS P2 and HSD P6 cells (not shown). Scale bar: 10 μm. (**B**) The number of migrated control cells (C1) in 10 1 $mm^2$ non-overlapping microscopic fields were counted for the different conditions: UM, C1 CM, cEDS P1 CM, hEDS CM (n = 2) and HSD CM (n = 2). Data represent the means ± SEM from 3 independent experiments performed in triplicate for the above groups (***P < 0.001 compared with C1 + UM). (**C**) IF of CCN1/CYR61 in 72 h-grown control C1, cEDS P1, hEDS P1, and HSD P5 cells. Scale bar: 10 μm. The images are representative of 2 control, 4 cEDS, 2 hEDS (P1, P2), and 2 HSD (P5, P6) cell strains (not shown). WB of 50 μg of proteins recovered from control C1, cEDS P1, hEDS P1 and P2, and HSD P5 and P6 CE and CM, immunoreacted with the rabbit anti-human CCN1/CYR61 Ab, detecting a 46 kDa band, and with rabbit anti-CTGF Ab, detecting a 37 kDa band. Loading control for CE: β-actin. (**D**) IF of FN-ECM analyzed in 72 h-grown control C1, cEDS P1, hEDS P1, and HSD P5 cells. The images are representative of 2 control, 4 cEDS, 2 hEDS (P1, P2), and 2 HSD (P5, P6) cell strains (not shown). IF of FN-ECM analyzed in control fibroblast (C1) grown for 10 days in the presence of its own CM (C1 + C1 CM), and CM recovered from cEDS P1 (C1 + cEDS P1 CM), hEDS P1 (C1 + hEDS P1 CM), and HSD P5 (C1 + HSD P5 CM) cells. Comparable results were obtained by using CM of hEDS P2 and HSD P6 cells (not shown). Scale bar: 10 μm. WB of 50 μg of proteins recovered from control C1, cEDS P1, hEDS P1 and P2, and HSD P5 and P6 cells' CM were immunoreacted with the anti-human FN Ab that detects a 250/260 kDa FN dimer. In hEDS and HSD cells' CM discrete fragments at 160, 110 and 60 kDa were present. WB was also performed with the anti-MMP-9 Ab, recognizing the 95 kDa pro-form and the 82 kDa active form of the enzyme. The relative mRNA expression levels of *MMP9* were determined with the $2^{-(\Delta\Delta Ct)}$ method. Bars represent the mean ratio of normalized target gene expression in hEDS (n = 4), HSD (n = 2, P5, P6) and cEDS (n = 4) *vs* control cells (n = 2). qPCR was performed in triplicate, and the results are expressed as mean ± SEM (*P < 0.05, **P < 0.01).

own CM and with that obtained from cEDS fibroblasts, showed ILK localization both in focal and fibrillar adhesions, whereas, after the treatment with CM from hEDS and HSD cells, ILK was mainly localized in focal adhesions, resembling its distribution in hEDS and HSD cells (Fig. 3B), in which co-localization with the β3 integrin subunit in focal adhesions was demonstrated (Fig. 3C). The organization of paxillin, a marker of both fibrillar and focal contacts, did not show any difference after treatment with the hEDS and HSD cells' CM, indicating that fibrillar sites are maintained in the presence of CM. Therefore, it is likely that the hEDS and HSD cells' media promote the ILK recruitment in focal adhesions through its interaction with the αvβ3 integrin, preferentially clustered in these sites only in the presence of hEDS and HSD cells' CM (Fig. 3A,D). These findings suggested a direct involvement in hEDS and HSD cells of an αvβ3/ILK-mediated signaling transduction pathway in the α-SMA cytoskeleton assembly. To validate this possibility, ILK was inhibited in control, hEDS, and HSD cells with increasing sublethal concentrations (0.5 to 2.0 μM) of the liposoluble ILK inhibitor Cpd22. In hEDS and HSD cells, the treatment with low amounts of Cpd22 (up to 2.0 μM) was associated both with the progressive reduction of αvβ3 integrin in fibrillar and focal adhesions and α-SMA cytoskeleton disassembly (Fig. 4), finally leading to cell detachment at 4.0 μM (not shown). In control fibroblasts, the treatment with increasing Cpd22 concentrations (up to 1 μM) induced the progressive localization of ILK in the focal adhesions and the concomitant organization of the αvβ3 integrin in these contacts along with the organization of α-SMA stress fibres (Fig. 4). Concentrations > 2.0 μM of Cpd22 induced cells' detachment (not shown). Taken together, these results reinforce the assumption that the ILK-αvβ3 complexes in focal contacts are essential to promote the α-SMA assembly that is indispensable for the myofibroblast differentiation.

### *3.4. The transcription factor Snail1/Slug is involved in the αvβ3-ILK-mediated signal transduction in hEDS and HSD myofibroblasts*

To identify downstream effectors of the αvβ3 integrin-ILK signal transduction in hEDS and HSD cells, the expression of the transcriptional repressor Snail1/Slug, known to be involved in cell motility and trans-differentiation mechanisms [32], was first analyzed by qPCR. As shown in **Supplementary Fig. 4**, hEDS and HSD cells expressed significantly higher levels of *SNAIL1* than control and cEDS fibroblasts. IF analysis showed that in hEDS and HSD cells the Snail1/Slug was localized both in the cytoplasm and nucleus; this distribution was not observed in control and cEDS fibroblasts (Fig. 5A). WB analyses confirmed that both total and nuclear Snail1/Slug were increased in hEDS and HSD cells compared to control and cEDS fibroblasts; in cEDS and control nuclei the transcription factor was almost undetectable (Fig. 5B). Furthermore, when compared to control fibroblasts, higher levels of Snail1/Slug co-immunoprecipitated from hEDS and HSD cells' extracts both with αvβ3 integrin (Fig. 3B) and with ILK (**Supplementary Fig. 5**). These data allow to hypothesize that in these cells Snail1/Slug, through an ILK-mediated interaction with the αvβ3 integrin, participates in the phenotypic switch of hEDS and HSD fibroblasts. To corroborate that in hEDS and HSD cells the higher Snail1/Slug nuclear expression associates with an αvβ3/ILK-mediated signal transduction, the distribution of this transcription factor was investigated, by IF and WB, after ILK inhibition with increasing sublethal concentrations of Cpd22. After treatment of hEDS and HSD cells with 0.5 to 2.0 μM Cpd22, total and nuclear Snail1/Slug gradually decreased (Fig. 5C). In contrast, in control fibroblasts the inhibition of ILK by low concentrations of Cpd22 (up to 1 μM), inducing the αvβ3 integrin and ILK localization in focal contacts and the α-SMA cytoskeleton assembly (Fig. 4), led to the cytoplasmic and nuclear Snail1/Slug up-regulation (Fig. 5C). Besides, control fibroblasts grown in the presence of hEDS and HSD cells' CM were induced to express and translocate into the nucleus Snail1/Slug (Fig. 5D). Overall, these data stand for the involvement of an αvβ3-ILK-Snail1/Slug axis in the hEDS and HSD cells' transdifferentiation mechanism.

## 4. Discussion

This study represents the first detailed cellular characterization of hEDS and HSD dermal fibroblasts and shed light on mechanisms associated with the molecular pathology of these genetically undefined disorders. Our findings suggest that hEDS and HSD are likely not distinct entities, but rather part of a phenotypic continuum characterized by a common altered tissue homeostasis and a chronic inflammatory condition. Indeed, both hEDS and HSD skin fibroblasts displayed *in vitro* the same disorganized ECM, a myofibroblast-like phenotype with the formation of α-SMA microfilaments, enhanced expression of OB-cadherin/cadherin-11 and MMP-9 together with an αvβ3-mediated signaling transduction pathway involving ILK and Snail1/Slug.

Disorganization of the ECM is a common feature of *in vitro* grown EDS fibroblasts [8–12] that should reflect both the dermal ultrastructural anomalies identified in different EDS types, such as irregular and loosely packed collagen fibrils [33,34], and the structural impairment of the numerous affected connective tissues, *i.e.*, joints, ligaments, tendon, skin, mucosae, muscle, and bone [4,35–37]. While for the genetically defined forms of EDS the ECM disarray and its secondary effects is explained by the underlying molecular defects, the responsible mechanism(s) in hEDS and related disorders remain(s) an enigma.

Our findings suggest that the increased expression of the active form of MMP-9 could explain the disassembly of the ECM and the fragmentation of FN observed in hEDS and HSD cells, at least in part since additional proteases might be involved. It is well established that ECM molecules or fragments released by MMPs modulate inflammatory/immune pathways and hyperalgesic signaling. Indeed, different ECM degradation products generated from hyaluronic acid, fibrinogen, and FN are included in damage-associated molecular patterns (DAMPs), which are released downstream of cell damage and injury [38–42]. COLLs, FN, and laminin fragments are known to have bioactive properties that regulate tissue remodeling [43], and MMP-9 plays a role in the ECM degradation in a large spectrum of physiologic and

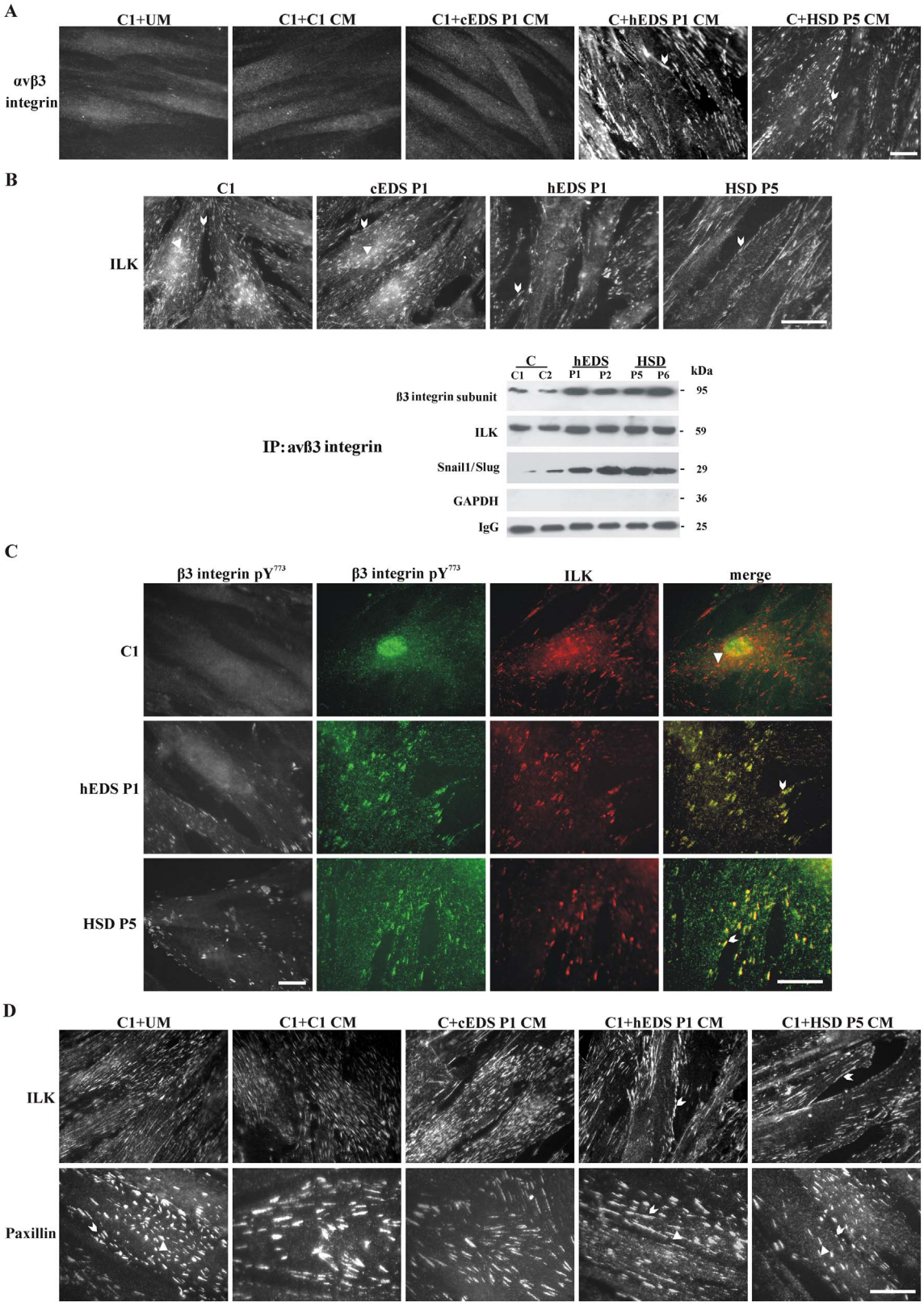


*(caption on next page)*

pathophysiologic processes [44]. For instance, MMP-9 expression stimulates cardiac fibroblasts migration and induces fibroblast-to-myofibroblast transition, essential in tissue remodeling and healing [45,46]. MMP-9-mediated proteolysis also stimulates the immune response to initiate pathogenesis or exacerbate disease progression. FN fragments generated by MMP-9 cleavage act as chemoattractants for a variety of cell types, including neutrophils and macrophages [47]. MMP-9 also processes several cytokines, including TNF-α, IL-1β, and the latent proform of TGF-β to its active state [44]. In line with these observations, our previous transcriptome analysis of hEDS and HSD fibroblasts

**Fig. 3. hEDS and HSD myofibroblasts secrete factors promoting the αvβ3 integrin and ILK recruitment in control cell's focal adhesions** (**A**) IF of αvβ3 integrin in control fibroblasts (C1) grown for 10 days in the presence of UM (C1 + UM), their own CM (C1 + C1 CM) and recovered from cEDS P1 (C1 + cEDS P1 CM), hEDS P1 (C1 + hEDS P1 CM), and HSD P5 (C1 + HSD P5 CM) cells. Comparable results were obtained by using CM of hEDS P2 and HSD P6 cells (not shown). Arrows indicate examples of focal adhesions that are integrin-containing structures localized on the lower and peripheral fibroblast surface conferring cell adhesion to the substrate; triangles indicate examples of fibrillar adhesions that are integrin-containing complexes localized on the upper cell surface involved in the ECM fibrils organization. Scale bar: 10 μm. (**B**) IF of ILK analyzed in 72 h-grown control C1, cEDS P1, hEDS P1, and HSD P5 cells. Scale bar: 10 μm. The images are representative of 2 control, 4 cEDS, 2 hEDS, and 2 HSD cell strains (not shown). WB of the αvβ3 integrin immunoprecipitated from 2 control, 2 hEDS (P1, P2), and 2 HSD (P5, P6) cell strains using an anti-αvβ3 integrin mAb, immunoreacted with the anti-β3 integrin subunit Ab, and anti-ILK mAb, detecting bands at 95 and 59 kDa, respectively, and with anti-Snail1/Slug Ab, detecting a 29 kDa band. Negative control of the immunoprecipitation: GAPDH. Loading control: IgG. (**C**) IF of the β3 integrin subunit phosphorylated in tyrosine 773 residue (β3 integrin $pY^{773}$) and its co-localization with ILK in 72 h-grown control C1, hEDS P1, and HSD P5 cells. The black/white and color images were captured from different fields for each cell strain. Scale bars: 10 μm. (**D**) IF of ILK and paxillin in control fibroblast (C1) grown for 10 days in the presence of UM (C1 + UM), its own CM (C1 + C1 CM), and CM recovered from cEDS P1 (C1 + cEDS P1 CM), hEDS P1 (C1 + hEDS P1 CM), and HSD P5 (C1 + HSD P5 CM) cells. Similar results were obtained by using CM of hEDS P2 and HSD P6 cells (not shown). Scale bar: 10 μm. (For interpretation of the references to color in this figure legend, the reader is referred to the web version of this article.)

revealed expression changes of several genes related to inflammatory and immune responses [8]. Furthermore, in hEDS and HSD patients' sera increased levels of different complement system proteins have been demonstrated, suggesting the possibility of locally occurring inflammatory processes [48]. All these data allow to hypothesize that hEDS and HSD patients share many characteristics with those affected by CID [7]. Fragments of FN and possibly of other ECM proteins might act as DAMPs in hEDS and HSD cells, likely contributing to the generation of the *in vitro* inflammation-like phenotype, which could be related to the chronic pain observed in hEDS and HSD patients [49].

Skin fibroblasts isolated from hEDS and HSD patients show a persistent *in vitro* phenotype characterized by synthesis and organization of α-SMA in cytoskeletal stress fibres that is observed neither in cEDS and vEDS nor in control skin fibroblasts. Besides, these cells show an increased migratory capability, that is, together with the MMPs-mediated proteolytic degradation of ECM and the α-SMA cytoskeleton assembly, a peculiar feature of a fibroblast-to-myofibroblast transition [50–52]. Our findings suggest that a proteolytic activity present in the CM of hEDS/HSD cells might be involved in the establishment of the myofibroblast-like phenotype. Indeed, when control fibroblasts are grown in the presence of CM of hEDS and HSD cells their abundant FN-ECM scaffold is disassembled and the α-SMA cytoskeleton is organized. Furthermore, the CM of hEDS and HSD fibroblasts enhances the migratory capability of control cells, resembling the hEDS and HSD myofibroblast-like phenotype.

The myofibroblast differentiation and the expression of α-SMA are regulated by different pathways, including TGF-β and Wnt/β-catenin signaling [53,54]. In particular, the treatment of fibroblasts with Wnt3a promotes the formation of a myofibroblast-like phenotype by up-regulating TGF-β signaling through SMAD2 in a canonical Wnt/β-catenin-dependent manner [54]. Conversely, blocking of Wnt/β-catenin signaling by the secreted frizzled-related protein 2 (sFRP2) prevents TGF-β-dependent myofibroblasts formation and myocardial fibrosis [55]. Interestingly, the possible involvement in the hEDS and HSD pathogenesis of the Wnt/β-catenin pathway was suggested by our previous microarray study that showed altered expression of several related genes with the sFRP2-encoding transcript as the most down-regulated in hEDS and HSD patients' cells [8]. Additional functional work is required to investigate the contribution of Wnt/β-catenin and TGF-β signaling pathways in the establishment of the myofibroblast-like phenotype in hEDS and HSD cells.

During wound healing and tissue regeneration, fibroblasts are generally induced to express α-SMA and become myofibroblasts, until they undergo apoptosis [26]. CCN2/CTGF and CCN1/CYR61 are known to be key inflammatory mediators in the proliferation and resolution phases. CCN1/CYR61 is expressed in myofibroblasts of granulation tissue and it controls fibrosis through cell senescence. Furthermore, it down-regulates α-SMA expression and myofibroblasts' cell migration and promotes their apoptosis, thereby playing an antagonist function towards the proliferative phase of inflammation positively modulated by CCN2/CTGF [24,56]. In hEDS and HSD cells, the strong reduction of CCN1/CYR61 together with the higher synthesis of CCN2/CTGF might participate in the fibroblast-to-myofibroblast transition.

Recently, in patients with connective tissue manifestations and multiple associated symptoms like those observed in hEDS and HSD elevated basal serum tryptase levels were identified [57]. Tryptase is a serine protease considered an inflammatory mediator secreted by mast cells that degrades glycoproteins, such as FN [58], activates MMPs [59], and affects the *in vivo* and *in vitro* phenoconversion of fibroblasts to myofibroblasts [60,61]. Mast cells are a recent, thrilling topic in EDS research, and more work is needed to clarify if their activation plays a role in the pathogenesis of hEDS and HSD [5].

hEDS and HSD fibroblasts express and organize into the plasma membrane other markers of the fibroblast-to-myofibroblast transition, *i.e.*, OB-cadherin/cadherin-11 and αvβ3 integrin. In hEDS and HSD cells, the organization of OB-cadherin/cadherin-11 is consistent with our previously reported down-regulation of several genes belonging to the N-cadherin family [8]. The expression of OB-cadherin/cadherin-11 was reported in fibroblast-like synoviocytes to maintain the integrity of joint structures [62,63], and the switch from E- and N-cadherin to the mesenchymal OB-cadherin/cadherin-11 has been correlated with increased mobility of these cells and with the enhanced synthesis of MMPs [64,65], leading to the notion that OB-cadherin/cadherin-11 is involved in synovial inflammatory reactions. The hEDS and HSD myofibroblast-like phenotype shares several features with synoviocytes that have been described in many inflammatory diseases affecting different connective tissue structures, *i.e.*, ligaments, tendons, and joints [27,65].

The recruitment on the cell surface of the αvβ3 integrin has been described as a hallmark of myofibroblasts [50–52]. The αvβ3 integrin expression is a common trait in fibroblasts derived from all types of EDS [8–12,66]. In cEDS and vEDS fibroblasts, a survival role of αvβ3 integrin in the rescue from apoptosis induced by the ECM disassembly was reported [10], which should not be excluded in hEDS and HSD cells given the widespread ECM disarray ([8]; this work). For instance, in hEDS and HSD cells, the binding of αvβ3 integrin to a FN fragment might up-regulate a non-canonic signal transduction pathway allowing the escape from apoptosis. On the other hand, only in hEDS and HSD cells, but not in cEDS and vEDS fibroblasts, the αvβ3 integrin is associated with the myofibroblast-like phenotype. Furthermore, the evidence that control fibroblasts, which do not express this integrin in standard growth conditions ([9,10], this work), organize it preferentially in focal adhesions in the presence of hEDS and HSD CM corroborates the involvement of αvβ3 integrin in focal contacts in the transdifferentiation of fibroblasts into myofibroblasts.

Indeed, we demonstrated that the αvβ3 integrin, localized in focal adhesions of hEDS and HSD cells, is phosphorylated in tyrosine 773 and co-distributes with ILK, reinforcing the hypothesis that the signal transduction pathway in hEDS and HSD cells is different from that described in cEDS and vEDS fibroblasts, in which the αvβ3 integrin signals to paxillin and p60Src without involving ILK [10]. In the focal contacts of hEDS and HSD cells, the αvβ3 integrin-ILK complex should be specifically involved in the establishment of the myofibroblast-like phenotype, because of the undetectable organization of β1 integrin subunits in these cells. Finally, a further proof that in hEDS and HSD cells the αvβ3 integrin-ILK complex in focal contacts plays a key role in

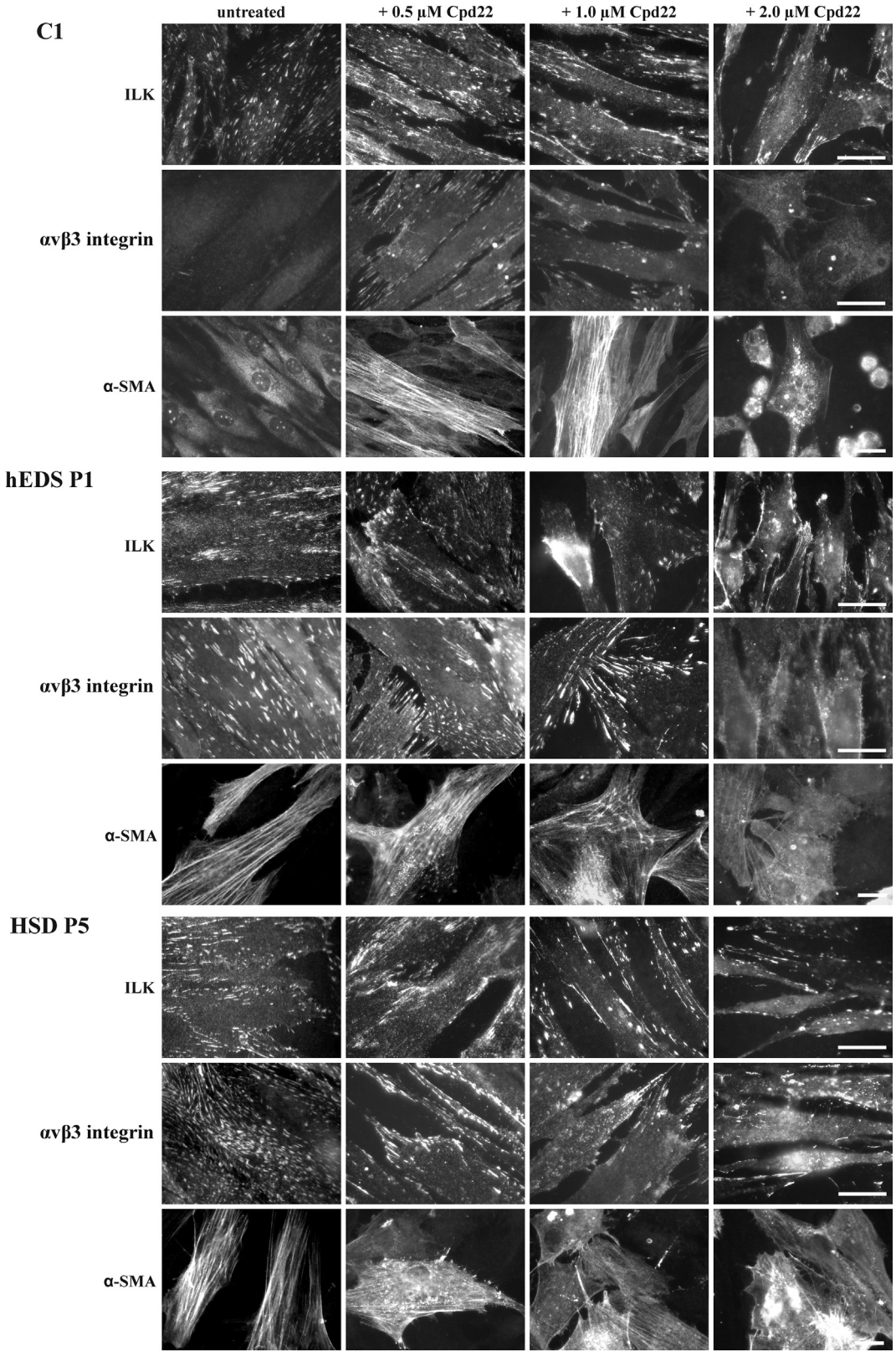


**Fig. 4. ILK in focal adhesions is essential for the α-SMA cytoskeleton assembly**. IF of ILK, αvβ3 integrin, and α-SMA analyzed in 18 h-grown control C1, hEDS P1, and HSD P5 cells in the absence and in the presence of increasing concentrations of ILK inhibitor-Cpd22 compound (0.5 to 2.0 μM). The images are representative of 2 control, 2 hEDS (P1, P2), and 2 HSD (P5, P6) cells (not shown). Scale bars: 10 μm.

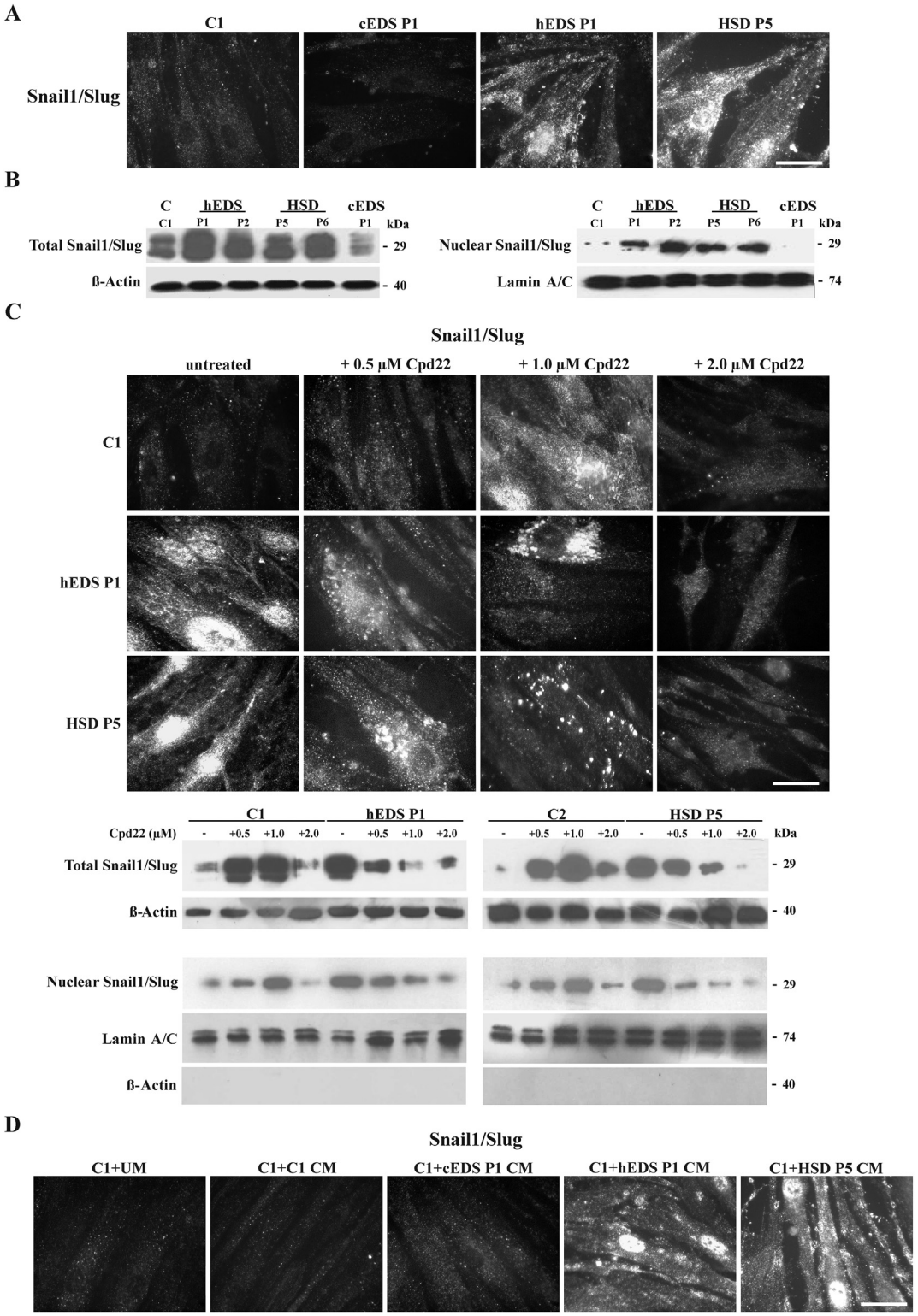


**Fig. 5. The transcription factor Snail1/Slug is involved in the αvβ3/ILK-mediated signal transduction for the α-SMA organization in hEDS and HSD myofibroblasts**. (**A**) IF of Snail1/Slug analyzed in 72 h-grown control C1, cEDS P1, hEDS P1, and HSD P5 cells. The images are representative of 2 control, 4 cEDS, 2 hEDS, and 2 HSD cell strains (data not shown). Scale bar: 10 µm. (**B**) WB of 25 µg of proteins recovered from control C1, cEDS P1, hEDS P1 and P2, and HSD P5 and P6 total and nuclear cells' extracts, immunoreacted with the rabbit anti-human Snail1/Slug Ab detecting a 29 kDa band. Loading control for total and nuclear extracts: β actin and lamin A/C, respectively. (**C**) IF of Snail1/Slug analyzed in 18 h-grown control C1, hEDS P1, and HSD P5 cells in the absence and in the presence of increasing concentrations of ILK inhibitor-Cpd22 compound (0.5 to 2.0 µM). The images are representative of 2 control, 2 hEDS, and 2 HSD cell strains (not shown). Scale bar: 10 µm. WB of 25 µg of proteins recovered from total and nuclear extracts of 18 h-grown control C1, C2, hEDS P1, and HSD P5 cells in the absence and in the presence of increasing concentrations of the ILK inhibitor Cpd22 (0.5 to 2.0 µM) and immunoreacted with the rabbit anti-human Snail1/Slug Ab detecting a 29 kDa band. Loading control for total and nuclear extracts: β-actin and lamin A/C, respectively. The nuclear extracts were also immunoreacted with the anti-β actin mAb to verify the purity of the cell fraction. The images are representative of 2 hEDS, and 2 HSD cell strains (not shown). (**D**) IF of Snail1/Slug in control fibroblast (C1) grown for 10 days in the presence of UM (C1 + UM), its own CM (C1 + C1 CM), and CM recovered from cEDS P1 (C1 + cEDS P1 CM), hEDS P1 (C1 + hEDS P1 CM), and HSD P5 (C1 + HSD P5 CM) cell strains. Comparable results were obtained by using CM of hEDS P2 and HSD P6 cells (not shown). Scale bar: 10 µm.

the acquisition of the myofibroblast-like phenotype was obtained by the disorganization of the α-SMA cytoskeleton observed after ILK inhibition that was associated with the gradual decrease of the αvβ3 integrin in these structures. This is confirmed by the fact that control fibroblasts, after treatment with the CM from hEDS and HSD cells, redistributed ILK in focal adhesions together with the concomitant recruitment of αvβ3 integrin, organized α-SMA in stress fibres and acquired a myofibroblast-like phenotype like that of hEDS and HSD cells.

ILK may act as a scaffold protein to function through cell-matrix interactions, cell signaling, and cytoskeletal organization. Proteins such as PINCH, α-parvin, β-parvin, and paxillin interact directly with ILK and facilitate its localization to focal adhesions and coordinate cell spreading and actin organization. ILK can also act as a kinase transmitting signals in a PI3K-dependent manner through several downstream effectors including AKT, GSK-3β, and NF-kB [31]. The inhibition of ILK signaling was shown to induce the up-regulation of E-cadherin and down-regulation of MMP-2 and MMP-9 expression, and other mesenchymal markers, such as N-cadherin, vimentin, and Snail1/Slug [67]. Among these numerous ILK-dependent targets, the nuclear transdifferentiation regulator Snail1/Slug is considered a key marker of the epithelial-to-mesenchymal transition. Snail1/Slug is up-regulated in activated fibroblasts in many diseases and pathologic lesions [31,32,68–75]. For instance, Snail1/Slug regulates the TNFα-mediated activation of synovial fibroblasts from patients with rheumatoid arthritis. On the other hand, overexpression of Snail1 in normal synovial fibroblasts was shown to induce myofibroblast markers such as OB-cadherin/cadherin-11 and α-SMA [76].

In hEDS and HSD cells the increased expression levels and nuclear accumulation of Snail1/Slug suggested a direct involvement of this transcriptional regulator in the establishment of the myofibroblast-like phenotype. This hypothesis was corroborated by the evidence that control fibroblasts, acquiring a myofibroblast-like phenotype by the treatment with the CM of hEDS and HSD cells, exhibited higher amounts of nuclear Snail1/Slug. As a further evidence, the inhibition of ILK with Cpd22 in hEDS and HSD cells not only led to the disorganization of the α-SMA cytoskeleton but also significantly reduced the nuclear accumulation of Snail1/Slug.

Cpd22 is known to abolish the ILK-mediated phosphorylation of AKT and GSK-3β [77]. Indeed, ILK by stimulating the AKT phosphorylation promotes NF-kB activation, which, in turn, binds the human Snail1 promoter leading to increased Snail transcription [31,68]. ILK-activated AKT also phosphorylates the β-catenin, leading to its nuclear accumulation and transcriptional activity which results in the expression of several genes typically associated with myofibroblasts including α-SMA [78]. Furthermore, ILK in focal adhesions can inactivate GSK-3β by phosphorylation allowing for the upregulation of Snail1 [31,67,79]. On the other hand, the active form of GSK-3β can phosphorylate Snail1/Slug at two consecutive motifs in serine-rich regions that control its subcellular localization and ubiquitination [80].

These ILK-dependent mechanisms might partially explain the results obtained by the inhibition of this kinase with low doses of Cpd22 both in hEDS and HSD cells and in control fibroblasts. In patients' cells, the loss of ILK in focal contacts should prevent the inactivation of GSK-3β, which results in the loss of Snail1's nuclear localization and its subsequent degradation, and the concomitant activation of AKT that, in turn, should result in the down-regulation of the β-catenin-dependent transcription of myofibroblast phenotype-related genes. On the contrary, in control cells Cpd22 treatment was associated with the preferential localization of ILK in focal adhesions that could lead to the inactivation by phosphorylation of GSK-3β, thus explaining the nuclear accumulation of Snail1. In addition, ILK in focal contacts could allow for the activation of AKT that, through β-catenin-dependent transcription regulation, leads to the acquisition of the α-SMA positive phenotype.

Both these potential molecular mechanisms could also occur when control fibroblasts are grown in the presence of hEDS and HSD cells' CM that also led to the preferential localization of ILK in focal contacts, where this kinase can act as a scaffold protein to promote α-SMA assembly and its incorporation into the cytoskeleton [31].

Although these signal transduction pathways downstream the αvβ3-ILK axis were not yet investigated at protein level, our previous microarray results indicated the perturbation of PI3K/AKT/GSK and NF-kB signaling in hEDS and HSD cells [8], suggesting a pivotal role of the αvβ3 integrin-ILK-mediated signal transduction in the fibroblast-to-myofibroblast transition.

Besides, increased Snail1/Slug levels have been also associated with the secretion of CCN2/CTGF, which, in turn, induces fibroblast-to-myofibroblast transition [81,82]. Moreover, the involvement of Snail1 in the MMP-9 expression has been reported [83,84]. Snail1 up-regulates expression of vimentin and MMPs, thereby leading to decreased cell adhesion and enhanced migration, whereas the targeting of *SNAIL1* expression by siRNA down-regulates the expression of the *MMP2* and *MMP9* [85,86]. Therefore, the involvement of Snail1/Slug in the up-regulated expression of MMP-9, acting in the hEDS and HSD fibroblast-to-myofibroblast transition, can be hypothesized.

In conclusion, this study reports the identification of a myofibroblast-like phenotype in dermal cells isolated both from hEDS and HSD patients, which distinguishes them from cEDS and vEDS fibroblasts, suggesting the presence of a common inflammatory-like state consistent with the patients' systemic clinical manifestations. Once confirmed on a larger number of hEDS and HSD patients' cell strains, this peculiar phenotype might be used as a cellular signature to support the clinical diagnosis of this(these) challenging disorder(s). The identification of the αvβ3 integrin-ILK-Snail1/Slug transduction pathway needs to be explored in depth to provide further insights into the molecular mechanisms involved in the pathophysiology of this(these) neglected disorder(s) and may represent a starting point for identifying potential therapeutic options.

Supplementary data to this article can be found online at https://doi.org/10.1016/j.bbadis.2018.01.005.

## Competing interests

The authors declare that they have no conflict of interest.

## Author contribution

Conceiving the study: NZ, MC. Collecting patients: MC. Experimental and statistical analyses: SB, NZ, NC, MR. All the authors participated in discussion and writing the manuscript. All the authors approved the submission of the manuscript in its present form.

## Funding

This research did not receive any specific grant from funding agencies in the public, commercial, or not-for-profit sectors.

## Transparency document

The Transparency document associated with this article can be found in online version.

## Acknowledgement

The authors thank the patients and their families for their kind availability for this study and the Fazzo Cusan family for its generous support.

## References

[1] F. Malfait, C. Francomano, P. Byers, J. Belmont, B. Berglund, J. Black, L. Bloom, J.M. Bowen, A.F. Brady, N.P. Burrows, M. Castori, H. Cohen, M. Colombi,

S. Demirdas, J. De Backer, A. De Paepe, S. Fournel-Gigleux, M. Frank, N. Ghali, C. Giunta, R. Grahame, A. Hakim, X. Jeunemaitre, D. Johnson, B. Juul-Kristensen, I. Kapferer-Seebacher, H. Kazkaz, T. Kosho, M.E. Lavallee, H. Levy, R. Mendoza-Londono, M. Pepin, F.M. Pope, E. Reinstein, L. Robert, M. Rohrbach, L. Sanders, G.J. Sobey, T. Van Damme, A. Vandersteen, C. van Mourik, N. Voermans, N. Wheeldon, J. Zschocke, B. Tinkle, The 2017 international classification of the Ehlers-Danlos syndromes, Am. J. Med. Genet. C: Semin. Med. Genet. 175 (2017) 8–26.

[2] P. Beighton, A. De Paepe, B. Steinmann, P. Tsipouras, R.J. Wenstrup, Ehlers-Danlos syndromes: revised nosology, Villefranche, 1997. Ehlers-Danlos National Foundation (USA) and Ehlers-Danlos Support Group (UK), Am. J. Med. Genet. 77 (1998) 31–37.

[3] R. Grahame, H.A. Bird, A. Child, The revised (Brighton 1998) criteria for the diagnosis of benign joint hypermobility syndrome (BJHS), J. Rheumatol. 27 (2000) 1777–1779.

[4] M. Castori, B. Tinkle, H. Levy, R. Grahame, F. Malfait, A. Hakim, A framework for the classification of joint hypermobility and related conditions, Am. J. Med. Genet. C: Semin. Med. Genet. 175 (2017) 148–157.

[5] B. Tinkle, M. Castori, B. Berglund, H. Cohen, R. Grahame, H. Kazkaz, H. Levy, Hypermobile Ehlers-Danlos syndrome (a.k.a. Ehlers-Danlos syndrome type III and Ehlers-Danlos syndrome hypermobility type): clinical description and natural history, Am. J. Med. Genet. C: Semin. Med. Genet. 175 (2017) 48–69.

[6] F.C. Henderson, C. Austin, E. Benzel, P. Bolognese, R. Ellenbogen, C.A. Francomano, C. Ireton, P. Klinge, M. Koby, D. Long, S. Patel, E.L. Singman, N.C. Voermans, Neurological and spinal manifestations of the Ehlers-Danlos syndromes, Am. J. Med. Genet. C: Semin. Med. Genet. 175 (2017) 195–211.

[7] R.H. Straub, C. Schradin, Chronic inflammatory systemic diseases: an evolutionary trade-off between acutely beneficial but chronically harmful programs, Evol. Med. Public Health 27 (2016) 37–51.

[8] N. Chiarelli, G. Carini, N. Zoppi, C. Dordoni, M. Ritelli, M. Venturini, M. Castori, M. Colombi, Transcriptome-wide expression profiling in skin fibroblasts of patients with joint hypermobility syndrome/Ehlers-Danlos syndrome hypermobility type, PLoS One 11 (2016) e0161347.

[9] N. Zoppi, R. Gardella, A. De Paepe, S. Barlati, M. Colombi, Human fibroblasts with mutations in COL5A1 and COL3A1 genes do not organize collagens and fibronectin in the extracellular matrix, down-regulate alpha2beta1 integrin, and recruit alphavbeta3 instead of alpha5beta1 integrin, J. Biol. Chem. 279 (2004) 18157–18168.

[10] N. Zoppi, S. Barlati, M. Colombi, FAK-independent alphavbeta3 integrin-EGFR complexes rescue from anoikis matrix-defective fibroblasts, Biochim. Biophys. Acta 1783 (2008) 1177–1188.

[11] M. Baumann, C. Giunta, B. Krabichler, F. Rüschendorf, N. Zoppi, M. Colombi, R.E. Bittner, S. Quijano-Roy, F. Muntoni, S. Cirak, G. Schreiber, Y. Zou, Y. Hu, N.B. Romero, R.Y. Carlier, A. Amberger, A. Deutschmann, V. Straub, M. Rohrbach, B. Steinmann, K. Rostásy, D. Karall, C.G. Bönnemann, J. Zschocke, C. Fauth, Mutations in FKBP14 cause a variant of Ehlers-Danlos syndrome with progressive kyphoscoliosis, myopathy, and hearing loss, Am. J. Hum. Genet. 90 (2012) 201–216.

[12] A.R. Janecke, B. Li, M. Boehm, B. Krabichler, M. Rohrbach, T. Müller, I. Fuchs, G. Golas, Y. Katagiri, S.G. Ziegler, W.A. Gahl, Y. Wilnai, N. Zoppi, H.M. Geller, C. Giunta, A. Slavotinek, B. Steinmann, The phenotype of the musculocontractural type of Ehlers-Danlos syndrome due to CHST14 mutations, Am. J. Med. Genet. A 170 (2016) 103–115.

[13] G. Parsonage, A.D. Filer, O. Haworth, G.B. Nash, G.E. Rainger, M. Salmon, C.D. Buckley, A stromal address code defined by fibroblasts, Trends Immunol. 26 (2005) 150–156.

[14] C.D. Buckley, D. Pilling, J.M. Lord, A.N. Akbar, D. Scheel-Toellner, M. Salmon, Fibroblasts regulate the switch from acute resolving to chronic persistent inflammation, Trends Immunol. 22 (2001) 199–204.

[15] R.T. Kendall, C.A. Feghali-Bostwick, Fibroblasts in fibrosis: novel roles and mediators, Front. Pharmacol. 5 (2014) 123.

[16] G. Gabbiani, The myofibroblast in wound healing and fibrocontractive diseases, J. Pathol. 200 (2003) 500–503.

[17] I. Kajihara, M. Jinnin, N. Honda, K. Makino, T. Makino, S. Masuguchi, K. Sakai, S. Fukushima, Y. Inoue, H. Ihn, Scleroderma dermal fibroblasts overexpress vascular endothelial growth factor due to autocrine transforming growth factor β signaling, Mod. Rheumatol. 23 (2013) 516–524.

[18] S.J. Flavell, T.Z. Hou, S. Lax, A.D. Filer, M. Salmon, C.D. Buckley, Fibroblasts as novel therapeutic targets in chronic inflammation, Br. J. Pharmacol. 153 (Suppl. 1) (2008) S241–246.

[19] J.J. Tomasek, J. McRae, G.K. Owens, C.J. Haaksma, Regulation of alpha-smooth muscle actin expression in granulation tissue myofibroblasts is dependent on the intronic CArG element and the transforming growth factor-beta1 control element, Am. J. Pathol. 166 (2005) 1343–1351.

[20] B. Hinz, Formation and function of the myofibroblast during tissue repair, J. Invest. Dermatol. 127 (2007) 526–537.

[21] B. Hinz, P. Pittet, J. Smith-Clerc, C. Chaponnier, J.J. Meister, Myofibroblast development is characterized by specific cell-cell adherens junctions, Mol. Biol. Cell 15 (2004) 4310–4320.

[22] J.J. Tomasek, G. Gabbiani, B. Hinz, C. Chaponnier, R.A. Brown, Myofibroblasts and mechano-regulation of connective tissue remodelling, Nat. Rev. Mol. Cell Biol. 3 (2002) 349–363.

[23] A. Pardo, M. Selman, Matrix metalloproteases in aberrant fibrotic tissue remodeling, Proc. Am. Thorac. Soc. 3 (2006) 383–388.

[24] L.F. Lau, CCN1/CYR61: the very model of a modern matricellular protein, Cell. Mol. Life Sci. 68 (2011) 3149–3163.

[25] I.A. Darby, N. Zakuan, F. Billet, A. Desmoulière, The myofibroblast, a key cell in normal and pathological tissue repair, Cell. Mol. Life Sci. 73 (2016) 1145–1157.

[26] I.A. Darby, B. Laverdet, F. Bonté, A. Desmoulière, Fibroblasts and myofibroblasts in wound healing, Clin. Cosmet. Investig. Dermatol. 7 (2014) 301–311.

[27] P.V. Kasperkovitz, T.C. Timmer, T.J. Smeets, N.L. Verbeet, P.P. Tak, L.G. van Baarsen, B. Baltus, T.W. Huizinga, E. Pieterman, M. Fero, G.S. Firestein, T.C. van der Pouw Kraan, C.L. Verweij, Fibroblast-like synoviocytes derived from patients with rheumatoid arthritis show the imprint of synovial tissue heterogeneity: evidence of a link between an increased myofibroblast-like phenotype and high-inflammation synovitis, Arthritis Rheum. 52 (2005) 430–441.

[28] M. Ritelli, C. Dordoni, M. Venturini, N. Chiarelli, S. Quinzani, M. Traversa, N. Zoppi, A. Vascellaro, A. Wischmeijer, E. Manfredini, L. Garavelli, P. Calzavara-Pinton, M. Colombi, Clinical and molecular characterization of 40 patients with classic Ehlers-Danlos syndrome: identification of 18 COL5A1 and 2 COL5A2 novel mutations, Orphanet J. Rare Dis. 8 (2013) 58.

[29] B. Drera, N. Zoppi, M. Ritelli, G. Tadini, M. Venturini, A. Wischmeijer, M.A. Nicolazzi, A. Musumeci, S. Penco, L. Buscemi, S. Crivelli, C. Danesino, M. Clementi, P. Calzavara-Pinton, S. Viglio, M. Valli, S. Barlati, M. Colombi, Diagnosis of vascular Ehlers-Danlos syndrome in Italy: clinical findings and novel COL3A1 mutations, J. Dermatol. Sci. 65 (2012) 77.

[30] K. Suzuki, P. Bose, R. Leong-Quong, D. Fujita, K. Riabowol, REAP: a two-minute cell fractionation method, BMC. Res. Notes 3 (2010) 294–299.

[31] G. Hannigan, A.A. Troussard, S. Dedhar, Integrin-linked kinase: a cancer therapeutic target unique among its ILK, Nat. Rev. Cancer 5 (2005) 51–63.

[32] N. Dave, S. Guaita-Esteruelas, S. Gutarra, Àlex Frias, M. Beltran, S. Peiró, A. García de Herreros, Functional cooperation between Snail1 and twist in the regulation of ZEB1 expression during epithelial to mesenchymal transition, J. Biol. Chem. 286 (2011) 12024–12032.

[33] I. Hausser, I. Anton-Lamprecht, Differential ultrastructural aberrations of collagen fibrils in Ehlers-Danlos syndrome types I–IV as a means of diagnostics and classification, Hum. Genet. 93 (1994) 394–407.

[34] T. Hermanns-Lê, M.A. Reginster, C. Piérard-Franchimont, P. Delvenne, G.E. Piérard, D. Manicourt, Dermal ultrastructure in low Beighton score members of 17 families with hypermobile-type Ehlers-Danlos syndrome, J Biomed Biotechnol 2012 (2012) 878107.

[35] C. Dordoni, M. Ritelli, M. Venturini, N. Chiarelli, L. Pezzani, A. Vascellaro, P. Calzavara-Pinton, M. Colombi, Recurring and generalized visceroptosis in Ehlers-Danlos syndrome hypermobility type, Am. J. Med. Genet. A 161 (2013) 1143–1147.

[36] R.H. Nielsen, C. Couppé, J.K. Jensen, M.R. Olsen, K.M. Heinemeier, F. Malfait, S. Symoens, A. De Paepe, P. Schjerling, S.P. Magnusson, L. Remvig, M. Kjaer, Low tendon stiffness and abnormal ultrastructure distinguish classic Ehlers-Danlos syndrome from benign joint hypermobility syndrome in patients, FASEB J. 28 (2014) 4668–4676.

[37] G. Mazziotti, C. Dordoni, M. Doga, F. Galderisi, M. Venturini, P. Calzavara-Pinton, R. Maroldi, A. Giustina, M. Colombi, High prevalence of radiological vertebral fractures in adult patients with Ehlers-Danlos syndrome, Bone 84 (2015) 88–92.

[38] D.L. Rosin, M.D. Okusa, Dangers within: DAMP responses to damage and cell death in kidney disease, J. Am. Soc. Nephrol. 22 (2011) 416–425.

[39] H.J. Anders, L. Schaefer, Beyond tissue injury-damage-associated molecular patterns, Toll-like receptors, and inflammasomes also drive regeneration and fibrosis, J. Am. Soc. Nephrol. 25 (2014) 1–14.

[40] M. Tajerian, J.D. Clark, The role of the extracellular matrix in chronic pain following injury, Pain 156 (2015) 366–370.

[41] J. Kato, C.I. Svensson, Role of extracellular damage-associated molecular pattern molecules (DAMPs) as mediators of persistent pain, Prog. Mol. Biol. Transl. Sci. 131 (2015) 251–279.

[42] R.E. Miller, A. Belmadani, S. Ishihara, P.B. Tran, D. Ren, R.J. Miller, A.M. Malfait, Damage-associated molecular patterns generated in osteoarthritis directly excite murine nociceptive neurons through Toll-like receptor 4, Arthritis Rheumatol. 67 (2015) 2933–2943.

[43] J. Trial, R.D. Rossen, J. Rubio, A.A. Knowlton, Inflammation and ischemia: macrophages activated by fibronectin fragments enhance the survival of injured cardiac myocytes, Exp. Biol. Med. (Maywood) 229 (2004) 538–545.

[44] A. Yabluchanskiy, Y. Ma, R.P. Iyer, M.E. Hall, M.L. Lindsey, Matrix metalloproteinase-9: many shades of function in cardiovascular disease, Physiology (Bethesda) 28 (2013) 391–403.

[45] Y. Wang, F. Xu, J. Chen, X. Shen, Y. Deng, L. Xu, J. Yin, H. Chen, F. Teng, X. Liu, W. Wu, B. Jiang, D.A. Guo, Matrix metalloproteinase-9 induces cardiac fibroblast migration, collagen and cytokine secretion: inhibition by salvianolic acid B from Salvia miltiorrhiza, Phytomedicine 19 (2011) 13–19.

[46] W.M.S. van den Borne, J. Diez, W. Matthijs Blankesteijn, J. Verjans, L. Hofstra, J. Narula, Myocardial remodeling after infarction: the role of myofibroblasts, Nat. Rev. Cardiol. 7 (2010) 30–37.

[47] R. Zamilpa, E.F. Lopez, Y.A. Chiao, Q. Dai, G.P. Escobar, K. Hakala, S.T. Weintraub, M.L. Lindsey, Proteomic analysis identifies *in vivo* candidate matrix metalloproteinase-9 substrates in the left ventricle post-myocardial infarction, Proteomics 10 (2010) 2214–2223.

[48] A. Watanabe, K. Satoh, T. Maniwa, K.I. Matsumoto, Proteomic analysis for the identification of serum diagnostic markers for joint hypermobility syndrome, Int. J. Mol. Med. 37 (2016) 461–467.

[49] M. Castori, S. Morlino, C. Celletti, G. Ghibellini, M. Bruschini, P. Grammatico, C. Blundo, F. Camerota, Re-writing the natural history of pain and related symptoms in the joint hypermobility syndrome/syndrome, hypermobility type, Am. J. Med. Genet. A 161 (2013) 2989–3004.

[50] B. Hinz, S.H. Phan, V.J. Thannickal, M. Prunotto, A. Desmoulière, J. Varga, O. De Wever, M. Mareel, G. Gabbian, Recent developments in myofibroblast biology:

paradigms for connective tissue remodeling, Am. J. Pathol. 180 (2012) 1340–1355.
[51] B. Hinz, Myofibroblasts, Exp. Eye Res. 142 (2016) 56–70.
[52] P. Bhattaram, U. Chandrasekharan, The joint synovium: a critical determinant of articular cartilage fate in inflammatory joint diseases, Semin. Cell Dev. Biol. 62 (2017) 86–93.
[53] A. Stempien-Otero, D.H. Kim, J. Davis, Molecular networks underlying myofibroblast fate and fibrosis, J. Mol. Cell. Cardiol. 97 (2016) 153–161.
[54] J.M. Carthy, F.S. Garmaroudi, Z. Luo, B.M. McManus, Wnt3a induces myofibroblast differentiation by upregulating TGF-beta signaling through SMAD2 in a beta-catenin-dependent manner, PLoS One 6 (2011) e19809.
[55] P. Blyszczuk, B. Müller-Edenborn, T. Valenta, E. Osto, M. Stellato, S. Behnke, K. Glatz, K. Basler, T.F. Lüscher, O. Distler, U. Eriksson, G. Kania, Transforming growth factor-β-dependent Wnt secretion controls myofibroblast formation and myocardial fibrosis progression in experimental autoimmune myocarditis, Eur. Heart J. 38 (2017) 1413–1425.
[56] E. Borkham-Kamphorst, C. Schaffrath, E. Van de Leur, U. Haas, L. Tihaa, S.K. Meurer, Y.A. Nevzorova, C. Liedtke, R. Weiskirchen, The anti-fibrotic effects of CCN1/CYR61 in primary portal myofibroblasts are mediated through induction of reactive oxygen species resulting in cellular senescence, apoptosis and attenuated TGF-β signaling, Biochim. Biophys. Acta 1843 (2014) 902–914.
[57] J.J. Lyons, X. Yu, J.D. Hughes, Q.T. Le, A. Jamil, Y. Bai, N. Ho, M. Zhao, Y. Liu, M.P. O'Connell, N.N. Trivedi, C. Nelson, T. DiMaggio, N. Jones, H. Matthews, K.L. Lewis, A.J. Oler, R.J. Carlson, P.D. Arkwright, C. Hong, S. Agama, T.M. Wilson, S. Tucker, Y. Zhang, J.J. McElwee, M. Pao, S.C. Glover, M.E. Rothenberg, R.J. Hohman, K.D. Stone, G.H. Caughey, T. Heller, D.D. Metcalfe, L.G. Biesecker, L.B. Schwartz, J.D. Milner, Elevated basal serum tryptase identifies a multisystem disorder associated with increased TPSAB1 copy number, Nat. Genet. 48 (2016) 1564–1569.
[58] J. Lohi, I. Harvima, J. Keski-Oja, Pericellular substrates of human mast cell tryptase: 72,000 dalton gelatinase and fibronectin, J. Cell. Biochem. 50 (1992) 337–349.
[59] J.B. Michel, Anoïkis in the cardiovascular system: known and unknown extracellular mediators, Arterioscler. Thromb. Vasc. Biol. 23 (2003) 2146–2154.
[60] A. Mangia, A. Malfettone, R. Rossi, A. Paradiso, G. Ranieri, G. Simone, L. Resta, Tissue remodelling in breast cancer: human mast cell tryptase as an initiator of myofibroblast differentiation, Histopathology 58 (2011) 1096–1106.
[61] J. MacLean, K.B. Pasumarthi, Signaling mechanisms regulating fibroblast activation, phenoconversion and fibrosis in the heart, Indian J. Biochem. Biophys. 51 (2014) 476–482.
[62] X. Valencia, J.M. Higgins, H.P. Kiener, D.M. Lee, T.A. Podrebarac, C.C. Dascher, G.F. Watts, E. Mizoguchi, B. Simmons, D.D. Patel, A.K. Bhan, M.B. Brenner, Cadherin-11 provides specific cellular adhesion between fibroblast-like synoviocytes, J. Exp. Med. 200 (2004) 1673–1679.
[63] H.P. Kiener, T. Karonitsch, The synovium as a privileged site in rheumatoid arthritis: cadherin-11 as a dominant player in synovial pathology, Best Pract. Res. Clin. Rheumatol. 25 (2011) 767–777.
[64] H.P. Kiener, B. Niederreiter, D.M. Lee, E. Jimenez-Boj, J.S. Smolen, M.B. Brenner, Cadherin 11 promotes invasive behavior of fibroblast-like synoviocytes, Arthritis Rheum. 60 (2009) 1305–1310.
[65] H.Y. Song, M.Y. Kim, K.H. Kim, I.H. Lee, S.H. Shin, J.S. Lee, J.H. Kim, Synovial fluid of patients with rheumatoid arthritis induces α-smooth muscle actin in human adipose tissue-derived mesenchymal stem cells through a TGF-β1-dependent mechanism, Exp. Mol. Med. 42 (2010) 565–573.
[66] N. Zoppi, M. Ritelli, M. Colombi, Type III and V collagens modulate the expression and assembly of EDA(+) fibronectin in the extracellular matrix of defective Ehlers-Danlos syndrome fibroblasts, Biochim. Biophys. Acta 1820 (2012) 1576–1587.
[67] C. FengYen, H. ShihWang, C. LongLee, S. KueiLiao, Roles of integrin-linked kinase in cell signaling and its perspectives as a therapeutic target, Gynecol. Minim. Inv. Ther. 3 (2014) 67–72.
[68] Y. Wu, B.P. Zhou, TNF-α/NF-κB/Snail pathway in cancer cell migration and invasion, Br. J. Cancer 102 (2010) 639–644.
[69] D. Gil, D. Ciołczyk-Wierzbicka, J. Dulińska-Litewka, P. Laidler, Integrin-linked kinase regulates cadherin switch in bladder cancer, Tumour Biol. 37 (2016) 15185–15191.
[70] E. Batlle, E. Sancho, C. Francí, D. Domínguez, M. Monfar, J. Baulida, A. García De Herreros, The transcription factor Snail is a repressor of E-cadherin gene expression in epithelial tumour cells, Nat. Cell Biol. 2 (2000) 84–89.
[71] C. Tan, P. Costello, J. Sanghera, D. Dominguez, J. Baulida, A.G. de Herreros, S. Dedhar, Inhibition of integrin linked kinase (ILK) suppresses beta-catenin-Lef/Tcf-dependent transcription and expression of the E-cadherin repressor, snail, in APC −/− human colon carcinoma cells, Oncogene 20 (2001) 133–140.
[72] P. Molina-Ortiz, A. Villarejo, M. MacPherson, V. Santos, A. Montes, S. Souchelnytskyi, F. Portillo, A. Cano, Characterization of the SNAG and SLUG domains of Snail2 in the repression of E-cadherin and EMT induction. Modulation by serine 4 phosphorylation, PLoS One 7 (2012) e36132.
[73] I. Serrano, P.C. McDonald, F.E. Lock, S. Dedhar, Role of the integrin-linked kinase (ILK)/Rictor complex in TGFβ-1-induced epithelial-mesenchymal transition (EMT), Oncogene 32 (2013) 50–60.
[74] M.A. Nieto, The ins and outs of the epithelial to mesenchymal transition in health and disease, Annu. Rev. Cell Dev. Biol. 27 (2011) 347–376.
[75] C. Chiang, K. Ayyanathan, Snail/Gfi-1 (SNAG) family zinc finger proteins in transcription regulation, chromatin dynamics, cell signaling, development, and disease, Cytokine Growth Factor Rev. 24 (2013) 123–131.
[76] S.Y. Chen, A.L. Shiau, Y.T. Li, C.C. Lin, I.M. Jou, M.F. Liu, C.L. Wu, C.R. Wang, Transcription factor snail regulates tumor necrosis factor α–mediated synovial fibroblast activation in the rheumatoid joint, Arthritis Rheumatol. 67 (2015) 39–50.
[77] S.L. Lee, E.C. Hsu, C.C. Chou, H.C. Chuang, L.Y. Bai, S.K. Kulp, C.S. Chen, Identification and characterization of a novel integrin-linked kinase inhibitor, J. Med. Chem. 54 (2011) 6364–6374.
[78] L.S. Verjee, J.S. Verhoekx, J.K. Chan, T. Krausgruber, V. Nicolaidou, D. Izadi, D. Davidson, M. Feldmann, K.S. Midwood, J. Nanchahal, Unraveling the signaling pathways promoting fibrosis in Dupuytren's disease reveals TNF as a therapeutic target, Proc. Natl. Acad. Sci. U. S. A. 110 (2013) E928–937.
[79] S.J. Serrano-Gomez, M. Maziveyi, M.S.K. Alahari, Regulation of epithelial-mesenchymal transition through epigenetic and post-translational modifications, Mol. Cancer 15 (2016) 18.
[80] B.P. Zhou, J. Deng, W. Xia, J. Xu, Y.M. Li, M. Gunduz, M.C. Hung, Dual regulation of Snail by GSK-3beta-mediated phosphorylation in control of epithelial-mesenchymal transition, Nat. Cell Biol. 6 (2004) 931–940.
[81] S.W. Lee, J.Y. Won, W.J. Kim, J. Lee, K.H. Kim, S.W. Youn, J.Y. Kim, E.J. Lee, Y.J. Kim, K.W. Kim, H.S. Kim, Snail as a potential target molecule in cardiac fibrosis: paracrine action of endothelial cells on fibroblasts through snail and CTGF axis, Mol. Ther. 21 (2013) 1767–1777.
[82] K. Wójcik-Pszczoła, B. Jakieła, H. Plutecka, P. Koczurkiewicz, Z. Madeja, M. Michalik, M. Sanak, Connective tissue growth factor regulates transition of primary bronchial fibroblasts to myofibroblasts in asthmatic subjects, Cytokine S1043-4666 (2017) 30261–30262.
[83] G.M. Shi, A.W. Ke, J. Zhou, X.Y. Wang, Y. Xu, Z.B. Ding, R.P. Devbhandari, X.Y. Huang, S.J. Qiu, Y.H. Shi, Z. Dai, X.R. Yang, G.H. Yang, J. Fan, CD151 modulates expression of matrix metalloproteinase 9 and promotes neoangiogenesis and progression of hepatocellular carcinoma, Hepatology 52 (2010) 183–196.
[84] B. Qiao, N.W. Johnson, J. Gao, Epithelial-mesenchymal transition in oral squamous cell carcinoma triggered by transforming growth factor-ß1 is Snail family-dependent and correlates with matrix metalloproteinase-2 and -9 expressions, Int. J. Oncol. 37 (2010) 663–668.
[85] S. Mikami, K. Katsube, M. Oya, M. Ishida, T. Kosaka, R. Mizuno, M. Mukai, Y. Okada, Expression of snail and slug in renal cell carcinoma: E-cadherin repressor snail is associated with cancer invasion and prognosis, Lab. Investig. 91 (2011) 1443–1458.
[86] S. Mikami, M. Oya, R. Mizuno, T. Kosaka, M. Ishida, N. Kuroda, Y. Nagashima, K. Katsube, Y. Okada, Recent advances in renal cell carcinoma from a pathological point of view, Pathol. Int. 66 (2016) 481–490.